Pergamon

Journal of Atmospheric and Terrestrial Physics, Vol. 58, No. 13, pp. 1421–1447, 1996

0021-9169/96 $15.00+0.00

0021-9169(95)00122-0

Empirical wind model for the upper, middle and lower atmosphere

A. E. Hedin,[1] E. L. Fleming,[2] A. H. Manson,[3] F. J. Schmidlin,[4] S. K. Avery,[5] R. R. Clark,[6] S. J. Franke,[7] G. J. Fraser,[8] T. Tsuda,[9] F. Vial[10] and R. A. Vincent[11]

[1]Goddard Space Flight Center, Greenbelt, MD 20771, U.S.A.; [2]Applied Research Corporation, Landover, MD 20771, U.S.A.; [3]University of Saskatchewan, Saskatoon, SK S7N 0W0, Canada; [4]Goddard Space Flight Center, Wallops Flight Facility, Wallops Island, VA 23337, U.S.A.; [5]University of Colorado, Boulder, CO 80309, U.S.A.; [6]University of New Hampshire, Durham, NH 03824, U.S.A.; [7]University of Illinois, Urbana, IL 62801, U.S.A.; [8]University of Canterbury, Christchurch, New Zealand; [9]Kyoto University, Kyoto, Japan; [10]Ecole Polytechnique, 91128, Palaiseau Cedex, France; [11]University of Adelaide, Adelaide, SA 5001, Australia

(*Received* 17 *April* 1995; *accepted in revised form* 26 *April* 1995)

Abstract—The HWM90 thermospheric wind model has been revised in the lower thermosphere and extended into the mesosphere, stratosphere and lower atmosphere to provide a single analytic model for calculating zonal and meridional wind profiles representative of the climatological average for various geophysical conditions. Gradient winds from CIRA-86 plus rocket soundings, incoherent scatter radar, MF radar, and meteor radar provide the data base and are supplemented by previous data driven model summaries. Low-order spherical harmonics and Fourier series are used to describe the major variations throughout the atmosphere including latitude, annual, semiannual, local time (tides), and longitude (stationary wave 1), with a cubic spline interpolation in altitude. The model represents a smoothed compromise between the original data sources. Although agreement between various data sources is generally good, some systematic differences are noted, particularly near the mesopause. Overall root mean square differences between data and model values are on the order of 15 m/s in the mesosphere and 10 m/s in the stratosphere for zonal winds, and 10 m/s and 5 m/s respectively for meridional winds. Copyright © 1996 Published by Elsevier Science Ltd.

INTRODUCTION

The recently published Cospar International Reference Atmosphere (CIRA 1986 or CIRA-86) contains monthly tabulations of zonal mean wind from 0 to 120 km (Fleming *et al.*, 1990) derived from a tropospheric climatology by Oort (1983) and use of the gradient wind approximation with the temperature and pressure tables derived from satellite remote sensing data by Barnett and Corney (1985) for the middle atmosphere and the mass spectrometer and incoherent scatter (MSIS-83) empirical model (Hedin, 1983) for the thermosphere. The MSIS-83 model was the predecessor of the MSIS-86 model (Hedin, 1987) model which constitutes the thermospheric portion of the CIRA-86 density and temperature model (Hedin, 1988).

The CIRA-86 tabulations are the successor to CIRA 1972 (CIRA-72) which contained wind tabulations (Groves, 1972a) based largely on rocket and some radar measurements. However, the CIRA-86 tabulations were derived independently of the prior rocket data or tabulated models. Monthly wind models for the upper mesosphere and lower thermosphere based entirely on MF (medium frequency) and meteor radar data have also been prepared (Miyahara *et al.*, 1991).

Thermospheric wind data from satellites and ground based incoherent scatter radar and Fabry–Perot optical interferometers have been combined (Hedin *et al.*, 1991) to generate an analytic empirical horizontal wind model (HWM90) of winds above 100 km using a limited set of vector spherical harmonics to describe spatial and temporal variations in the exosphere and at selected altitude nodes with cubic spline interpolation between nodes. The formulation of this wind model is analogous to the MSIS-86 density and temperature model and allows the user to obtain atmospheric parameters at an arbitrary location and time. The MSIS-86 model was recently extended (Hedin, 1991) into the lower atmosphere to provide a single analytic reference model [MSISE-90] of temperature and density from the ground to the exosphere. While the lower atmosphere portion was

essentially derived from the CIRA-86 tabulations, the structure in the upper mesosphere was adjusted to best fit historical rocket data as well as maintain overall hydrostatic equilibrium, while smoothly joining the previous upper thermosphere model.

It is the goal of the HWM93 model described herein to extend the formulation of the HWM90 wind model into the mesosphere and down to the surface so as to provide a description of the average (climatological) wind system throughout the atmosphere and tidal (local time) variations in the stratosphere and mesosphere. The model is based not only on the CIRA-86 tabulations, but selected historical rocket data, previous rocket data based tabulations, meteor radar and MF radar data, and lower thermosphere incoherent scatter data previously used for HWM90. The new model thus represents a compromise between data sources in the upper stratosphere, mesosphere, and lower thermosphere, while closely following CIRA-86 in the lower stratosphere and troposphere and HWM90 in the thermosphere. Model results and data comparisons are given with emphasis on the mesosphere and lower thermosphere, and include also gradient winds calculated from MSISE-90 and theoretical semidiurnal winds calculated from Forbes and Vial (1989). The HWM90 model parameters were changed at 100 km to provide a smoother transition into the mesosphere but otherwise remain unchanged in the thermosphere.

DATA SOURCES

The data used to generate this model were derived from published tabulations, figures, and original data bases as summarized in Table 1. The number and diversity of data sources is greatest in the mesosphere and lower thermosphere consistent with availability and the emphasis of this paper.

In the mesosphere and lower thermosphere the techniques and sources represented include incoherent scatter radar, MF radar, meteor radar, rocketsondes, rocket grenade soundings, and gradient winds. The radar and rocket data were given the most weight in deriving the zonal mean model. Although MF radar data appear in later plots at their nominal attributed altitude, they were given considerably less weight in the fit above 100 km because their real and apparent altitudes are different near the total reflection height. In addition, tabulations in CIRA-72 (Groves, 1972a), GROVES-69 (Groves, 1969), and CAO-83 (Central Aerological Observatory) (Koshelkov, 1983) summarizing largely older or different rocket data and tabulations from CIRA-86 (Fleming *et al.*, 1990), providing global coverage largely based on gradient wind calculations, were included with approximately a factor of two less weight than the rocket and radar data. Gradient winds derived from MSISE-90 were weighted a factor of ten less than the rocket and radar data and thus are only included for comparison purposes below 85 km. However, the CIRA-86 winds were weighted less above 85 km by a factor of sixteen in order to give some precedence to the newer MSISE-90 representation of the mesosphere/thermosphere transition region. The model is thus primarily determined by the relatively recent direct radar and rocket wind measurements and to a lesser degree (except where direct measurements are unavailable) by CIRA and other tabulated summaries in the stratosphere and mesosphere and by MSIS-90 gradient winds in the lower thermosphere.

In the stratosphere the data include rocketsondes, and rocket grenade soundings, CIRA-72, CAO-83, tabulations from CIRA-86 and MSISE-90 gradient winds (Table 1). The direct measurements, when available, play the most important role in the model as discussed above. For the troposphere, only the CIRA-86 tabulations and MSISE-90 gradient winds are used. While the data sources are largely independent, there are also significant overlaps which should be kept in mind. The data sets will now be described with this aspect in mind as far as is known.

Unlike earlier CIRA tabulations, the CIRA-86 reference atmosphere winds in the stratosphere and mesosphere are derived from satellite remote sounding pressure and temperature data and a thermospheric density and temperature model and make no direct use of rocket or radar wind data. The CIRA-86 winds were largely derived from the gradient wind equation. However, equatorial winds were based on the second derivative of pressure where the geostrophic formulation fails; tropospheric winds were based on a published data summary (Oort, 1983); and very high latitude winds were based on a dynamical constraint (see Fleming *et al.*, 1990). For longitudinal variations of the prevailing zonal and meridional wind, the CIRA-86 tabulations were supplemented with gradient wind calculations derived from zonal wave 1 amplitudes and phases of geopotential height (Fleming *et al.*, 1990). These gradient winds were favorably compared with radar derived winds by Manson *et al.* (1991) at altitudes below 85 km. Gradient winds (including equatorial winds using the second derivative formulation) were also derived from the MSISE-90 density and temperature model and will be similar to the CIRA-86 winds, since MSISE-90 is based heavily on the same CIRA-86 pressure and temperature tabulations. However, there are differences, par-

Table 1. Wind data summary

Wind Station	Component	Latitude (deg)	Longitude (deg)	Years	Plot altitude (km)	Symbol	Reference
Incoherent Scatter							
EISCAT	M&Z	69.6N	19.2E	85–87	100–120	B	[Virdi and Williams, 1989][3]
Chatanika	M&Z	65.1N	147.4W	76–82	90–130	1	[Johnson *et al.*, 1987][3]
St. Santin	M	44.6N	2.2E	73–85	90–170	5	[Bernard, 1974][3]
Millstone	M&Z	42.5N	71.5W	76–77	105–135	3	[Wand, 1983][1]
Arecibo	M	18.3N	66.8W	74–77	100–170	6	[Harper *et al.*, 1976][3]
Arecibo	Z			74–75	100–130	6	[Harper, 1977][1]
MF radar, monthly averages							
Tromso*	M&Z	70N	20E	87–89	67–112	M	[Manson and Meek, 1991][2]
Saskatoon (mean)*	M&Z	52N	107W	79–82	61–111	F	[Manson *et al.*, 1981; Manson *et al.*, 1990][1]
Saskatoon (tides)*	M&Z	52N	107W	85	61–111	F	[Manson *et al.*, 1989][2]
Urbana	M&Z	40N	88W	91–92	66–111	T	[Franke and Thorsen, 1993][3]
Townsville	M&Z	20S	147E	78–80	70–100	K	[Vincent and Ball, 1981; Manson *et al.*, 1990][1]
Adelaide (mean)	M&Z	35S	138E	78–86	70–100	J	[Vincent and Stubbs, 1977; Manson *et al.*, 1990][1]
Adelaide (tides)	M&Z	35S	138E	84–86	70–100	J	[Vincent *et al.*, 1988][2]
Christchurch (mean)	M&Z	44S	173E	78–80	65–102	I	[Manson *et al.*, 1990][1]
Christchurch (tides)	M&Z	44S	173E	79	65–102	I	[Fraser, 1990; Manson *et al.*, 1989][2]
Mawson	M&Z	67.6S	62.9E	84–86	76–108	O	[MacLeod and Vincent, 1985; Manson *et al.*, 1981][1]
Meteor radar, monthly averages							
Poker Flat (mean)	M&Z	65N	147W	83–84	75–106	W	[Avery *et al.*, 1983; Manson *et al.*, 1990][1]
Poker Flat (tides)	M&Z	65N	147W	83–84	75–106	W	[Avery *et al.*, 1983][2]
Garchy (mean)	Z	47N	3E	70–76	78–102	+	[Massebeuf *et al.*, 1979][2]
Garchy (tides)	Z	47N	3E	79	78–102	+	[Massebeuf *et al.*, 1979; Manson *et al.*, 1989][2]
Monpazier (mean)	Z	44N	1E	79–80	76–104	L	[Massebeuf *et al.*, 1981; Manson *et al.*, 1990][1]
Monpazier (tides)	Z	44N	1E	79–80	76–104	L	[Bernard *et al.*, 1981; Manson *et al.*, 1989][2]
Durham (mean)	M&Z	43N	71W	78–84	77–110	V	[Clark, 1983; Manson *et al.*, 1990][1]
Durham (tides)	M&Z	43N	71W	78–84	77–110	V	[Clark, 1983; Manson *et al.*, 1989][2]
Kyoto (mean)	M&Z	35N	136E	83–84	82–106	G	[Tsuda *et al.*, 1987; Manson *et al.*, 1985][1]
Kyoto (tides)	M&Z	35N	136E	83–84	82–106	G	[Tsuda *et al.*, 1987][2]
Atlanta (mean)	M&Z	34N	84W	74–77	80–100	H	[Salby and Roper, 1980; Manson *et al.*, 1990][1]
Punta Borinquen (mean)	Z	18N	67W	77–78	80–100	R	[Massebeuf *et al.*, 1981; Manson *et al.*, 1990][1]
Punta Borinquen (tides)	Z	18N	67W	77–78	80–100	R	[Bernard *et al.*, 1981][1]
Christmas Is.	M&Z	2N	158W	88–91	80–100	S	[Avery *et al.*, 1990][3]
Rocket data							
Grenade	M&Z			60–72	30–100	N	[Theon *et al.*, 1972][1]
Falling sphere	M&Z			69–91	25–100	P	[Schmidlin *et al.*, 1985][3]
Datasonde	M&Z			69–91	20–75	C	[Schmidlin, 1986][3]

Table 1—*continued.*

Wind Station	Component	Latitude (deg)	Longitude (deg)	Years	Plot altitude (km)	Symbol	Reference
Model tabulations							
CIRA-86 gradient wind	Z				0–120	8	[Fleming *et al.*, 1990][1]
Wave 1	M&Z				15–82	8	[Fleming *et al.*, 1988][3]
MSISE-90 gradient wind	Z				0–120	A	[Hedin, 1991]
Wave 1	M&Z				0–120	A	[Hedin, 1991]
CIRA-72	Z				25–130	9	[Groves, 1972a][1]
Groves-69	M				60–130	E	[Groves, 1969][1]
CAO southern hemisphere	Z			20–80	7		[Koshelkov, 1983][1]

Wind component is M, Z, or M&Z for meridional, zonal, or both.
* Ten day averages
[1] Data from published tabulations or plots.
[2] Data from MLT radar database
[3] Data from other original databases.

ticularly in the upper mesosphere/lower thermosphere, and these are greatest near the equator. Also, winds derived from the MSISE-90 model will have smoother variations as a function of latitude and month than the CIRA-86 tabulations since MSISE-90 represents a smoothed version of density and temperature variations.

The CIRA-72 zonal winds (no meridional winds were published) are largely determined by rocket wind data and early radio-meteor results available at that time. Much of the data was from reports and private sources not readily available today, but there is some overlap with rocket data used here. Below 60 km there are separate tables for American and European longitudes and these were taken to apply to 90°W and 20°E to represent the approximate longitude of the respective data locations.

The CAO-83 southern hemisphere reference tabulations (only zonal wind) are derived largely from Russian rocket data but probably overlap slightly the data used in CIRA-72. A later version (Koshelkov, 1990) incorporates more rocketsonde data but also radar data that are separately included here.

The GROVES-69 tabulations are an older version of CIRA-72 for both zonal and meridional winds and include some of the early rocket data. Only the meridional wind from these tabulations is used here since CIRA-72 superceded the zonal winds but did not include meridional wind.

Rocketsonde data from the Meteorological Rocket Network were obtained from the NASA/Wallops database, which is similar to the World Data Center format available from the National Climate Data Center at Asheville, N.C. The data cover the time period from 1969 to 1991 and were separated into falling sphere data (Schmidlin, 1986), which make useful measurements to nearly 100 km, and parachute/datasonde measurements which were limited to 75 km. Based on the available time period, only slight overlap is possible with CIRA-72. The MRN concentrated on taking data near local noon, but data are available for all parts of the day for most stations. For each station, the data at 2 km intervals were separated into two hour local time groups. Monthly averages, determined by summing over all available years, were formed separately for the 12 local time groups. These averages, which provide as equitable a local time coverage as possible, were used as the rocketsonde input to the model and data comparisons.

The rocket grenade data from 1960 to 1972 used here were partly included in GROVES-69 and CIRA-72, but are not part of the rocketsonde data set and were not averaged on a monthly basis.

The more recent MF and Meteor radar data included here were not available for CIRA-72, but are presented as supplementary data for CIRA 1986 (Manson *et al.*, 1990).

Model formulation

The HWM93 model is an extension of the HWM87 and HWM90 models (Hedin *et al.*, 1988, 1991) summarizing wind measurements in the thermosphere. Latitude, longitude, and local time variations in the horizontal wind vector are represented by an expan-

sion in vector spherical harmonics (Morse and Feshbach, 1953) with each expansion coefficient represented by a Fourier series in day of year for annual and semiannual variations. The expansion involves two orthogonal vector fields, the divergence B field and the rotational C field. Solar activity and magnetic activity variations are not included below 100 km. Hemispheric differences are represented only by the lowest order asymmetric harmonic because of the limited and uneven data coverage between hemispheres. Tidal and non-tidal variations were fit independently, but in an iterative fashion to produce as self-consistent an overall model as possible, and tidal variations were limited to above approximately 45 km. Quasi-biennial variations are not included. Zonally averaged meridional winds were not modeled below 45 km. Stationary wave 1 longitude variations were limited from 7 to 90 km due to lack of other data. Only the rotational (C) field was used to represent longitude variations since the winds are nearly geostrophic, and thus nearly non-divergent, and it seemed unlikely that departures from a curl field could be extracted from the current limited data. No longitude dependence of the tidal components was considered, given the lack of data coverage.

Below 100 km the wind profiles are represented by a cubic spline, defined by cubic polynomials between specified nodes with first and second derivatives continuous across interior nodes. The nodes were chosen to be at 100, 90, 82.5, 75, 67.5, 60, 52.5, 45, 37.5, 30, 22.5, 15, 7.5 and 0 km providing a convenient division into intervals of approximately one scale height. The wind magnitude and altitude gradient are matched at 100 km with the thermospheric values, and in addition the altitude gradient is specified (fit) at 100 km.

The harmonic expansion at each altitude node is limited to low order terms as summarized in Table 2 a and b, thus smoothing the model output in space and time. The classification into symmetrical and asymmetrical is with respect to reflection about the equator, with symmetrical meaning that the vector spherical harmonic term provides zonal winds which have the same direction either side of the equator while the meridional wind changes direction. The column value 'm' refers to the local time harmonic content (1 the first harmonic, etc.). The 'n' value is the latitude harmonic order and is always equal to or larger than 'm'. If the n minus m value is even, then the B field term is symmetric and the C field term is asymmetric. The higher the order 'n' the greater the latitude variability that can be represented. Only low order terms were used because of the sparse and uneven latitudinal distribution of measurement stations and the limited time series available covering different time periods for different stations. In Table 2 a dash (—) means this term is not included for this node.

The determination of the harmonic coefficients for the various nodes of the wind profile is accomplished by a least squares fit to selected subsets of the data. The node to node variations of the harmonic coefficients were smoothed by refitting with the sum of the squares of the differences between adjacent node coefficients (multiplied by a constant) added to the usual sums of squares of data minus model differences. The multiplicative (tension) constant was chosen so that the sums of squares of the data residuals increased by no more than 1%.

Root mean square deviations of the data from the model in different altitude regions are given in Tables 3a and b. The grenade and incoherent scatter data tend to have the largest average departures because they were not smoothed or based on monthly averages. Natural variability is also high in the upper mesosphere due to breaking gravity waves and in the lower thermosphere where electrodynamic effects are important.

MODEL EXAMPLES AND DISCUSSION

Zonal average zonal wind

Here we present examples of the model predictions and data comparisons. A larger number of model and comparison plots were presented by Hedin *et al.* (1993a). Latitudinal cross-sections are shown in Fig. 1 for four different months and describe basic features of the zonal circulation which are well documented in the literature (e.g. Angell and Korshover, 1970; Groves, 1972b; Belmont, 1985, and references therein). The annual variation of the zonal wind has a winter eastward (westerly) maximum phase, peaking at mid latitudes just above the stratopause, with amplitudes of 70 m/s (southern hemisphere) and 60 m/s (northern). An annual variation with a summer eastward maximum phase exists just above the mesopause with an amplitude of 10 m/s. The semiannual variation has an equinox eastward maximum at low latitudes, with an amplitude of 20 m/s in the upper stratosphere and a westward maximum at the equinoxes in the upper mesosphere with an amplitude of 15 m/s.

The annual average zonal winds from the model (not shown) are fairly similar to those in CIRA-86. They are mostly eastward in both hemispheres with peaks at 30 m/s at mid-latitudes in the southern hemisphere stratosphere (15 m/s in northern hemisphere). An equatorial zone of westward flow peaks near 15

Table 2. (a) Maximum B field spherical harmonic order (n)

Term	m	B field parameter (node altitude) 100	90	82	75	67	60	52	45	37	30	22	15	7	0	grad
100																
Symmetrical																
Time independent	0	4	4	4	4	4	2	2	2	—	—	—	—	—	—	2
Semiannual	0	—	2	2	2	2	2	2	—	—	—	—	—	—	—	—
Diurnal	1	5	5	5	5	3	3	3	3	—	—	—	—	—	—	3
Semidiurnal	2	4	4	4	4	4	4	4	4	—	—	—	—	—	—	4
Asymmetrical																
Annual	0	3	1	1	1	1	—	—	—	—	—	—	—	—	—	1
Diurnal	1	2	2	2	2	—	—	—	—	—	—	—	—	—	—	—
Diurnal-annual	1	2	2	2	2	—	—	—	—	—	—	—	—	—	—	—
Didiurnal	2	3	3	3	—	—	—	—	—	—	—	—	—	—	—	—
Semidiurnal-annual	2	3	3	3	3	—	—	—	—	—	—	—	—	—	—	—
Semidiurnal-semiannual	2	3	3	3	—	—	—	—	—	—	—	—	—	—	—	—

(b) Maximum C field spherical harmonic order (n)

Term	m	C field parameter (node altitude) 100	90	82	75	67	60	52	45	37	30	22	15	7	0	grad
100																
Symmetrical																
Time independent	0	5	5	5	5	5	5	5	5	5	5	5	5	5	5	5
Annual	0	—	1	1	1	1	1	1	1	1	1	1	1	—	—	—
Semiannual	0	3	5	5	5	5	5	5	5	5	5	3	3	—	—	3
Longitude	1	—	—	6	6	6	6	6	6	6	6	6	6	—	—	—
Longitude-annual	1	—	—	6	6	6	6	6	6	6	6	6	6	—	—	—
Longitude-semiannual	1	—	—	6	6	6	6	6	6	6	6	6	6	—	—	—
Diurnal	1	6	6	6	6	4	4	4	4	—	—	—	—	—	—	4
Semidiurnal	2	5	5	5	5	5	5	5	5	—	—	—	—	—	—	5
Diurnal	1	1	1	1	1	—	—	—	—	—	—	—	—	—	—	—
Diurnal-annual	1	1	1	1	1	—	—	—	—	—	—	—	—	—	—	—
Semidiurnal	2	2	2	2	—	—	—	—	—	—	—	—	—	—	—	—
Semidiurnal-annual	2	2	2	2	2	—	—	—	—	—	—	—	—	—	—	—
Semidiurnal-semiannual	2	2	2	2	—	—	—	—	—	—	—	—	—	—	—	—
Asymmetrical																
Time independent	0	—	—	—	2	2	2	2	2	2	2	2	2	2	2	—
Annual	0	4	6	6	6	6	6	6	6	6	6	6	6	6	6	2
Semiannual	0	—	4	4	4	4	4	4	4	4	4	4	—	—	—	—
Longitude	1	—	—	5	5	5	5	5	5	5	5	5	5	—	—	—
Longitude-annual	1	—	—	5	5	5	5	5	5	5	5	5	5	—	—	—
Longitude-semiannual	1	—	—	5	5	5	5	5	5	5	5	5<	5	—	—	—

m/s in the stratosphere with small zones near the surface and upper mesosphere. Eastward winds in the lower thermosphere of approximately 15 m/s are not as large as in CIRA-86, reflecting the smaller magnitudes measured by radar.

Examples of model wind altitude profiles and comparisons with data are shown in Figs 2–4 for annual averages. Here data have been selected for rather broad latitude intervals and the model wind plotted versus altitude for the midpoint of the selected intervals. The example model plot will represent the model prediction at the exact latitude of individual measurements with a degree of faithfulness that depends on how rapidly the model varies with altitude, latitude, etc. The difference between the plotted points and the model line represents the average difference of each measurement, separated by source as specified in Table 1, from the model (calculated exactly for that location), and the error bars represent the one standard deviation scatter of this difference within the plot bin limits. There are three plots for each situation, separating data into three groups: gradient winds, one as published in CIRA-86 and one as derived from MSISE-90; rocket data, CIRA-72, and CAO-83 (pri-

Table 3. RMS zonal wind differences from HWM92

Data set	15–60 km rms	15–60 km pts	60–90 km rms	60–90 km pts	90–120 km rms	90–120 km pts
MSIS Gradient	8	1428	12	1020	15	1020
CIRA-86	8	2521	13	1973	21	1825
Datasonde	7	4949	13	1694		
Falling Sphere	10	1550	13	1336	32	135
Grenade	16	771	18	973	55	146
CIRA-72	16	1655	18	1225	22	744
CAO-83	10	768	12	480		
MF radar			6	1029	6	896
Meteor radar			11	776	8	866
IS radar	47	1329				
RMS meridional wind differences from HWM92						
Datasonde	4	4949	9	1684		
Falling Sphere	4	1551	9	1368	27	138
Grenade	10	772	16	973	50	147
GROVES-69	5	204	8	1260	12	972
MF radar			5	1028	5	896
Meteor radar			9	394	6	487
IS radar	34	2064				

Here rms is root mean square difference between data and model, pts is number of sample points, MF is medium frequency, and IS is incoherent scatter.

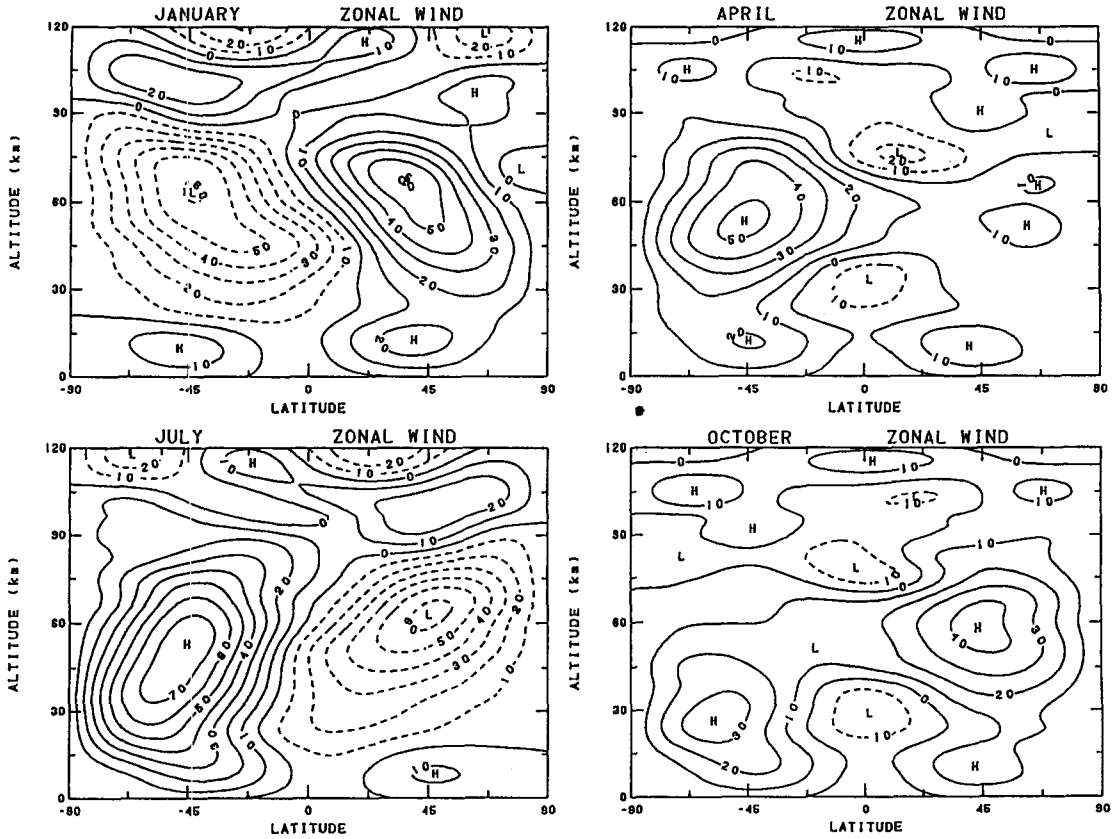

Fig. 1. Contour plots in altitude versus latitude of the DL (diurnal and longitudinal) average zonal wind for four indicated months (mid-month).

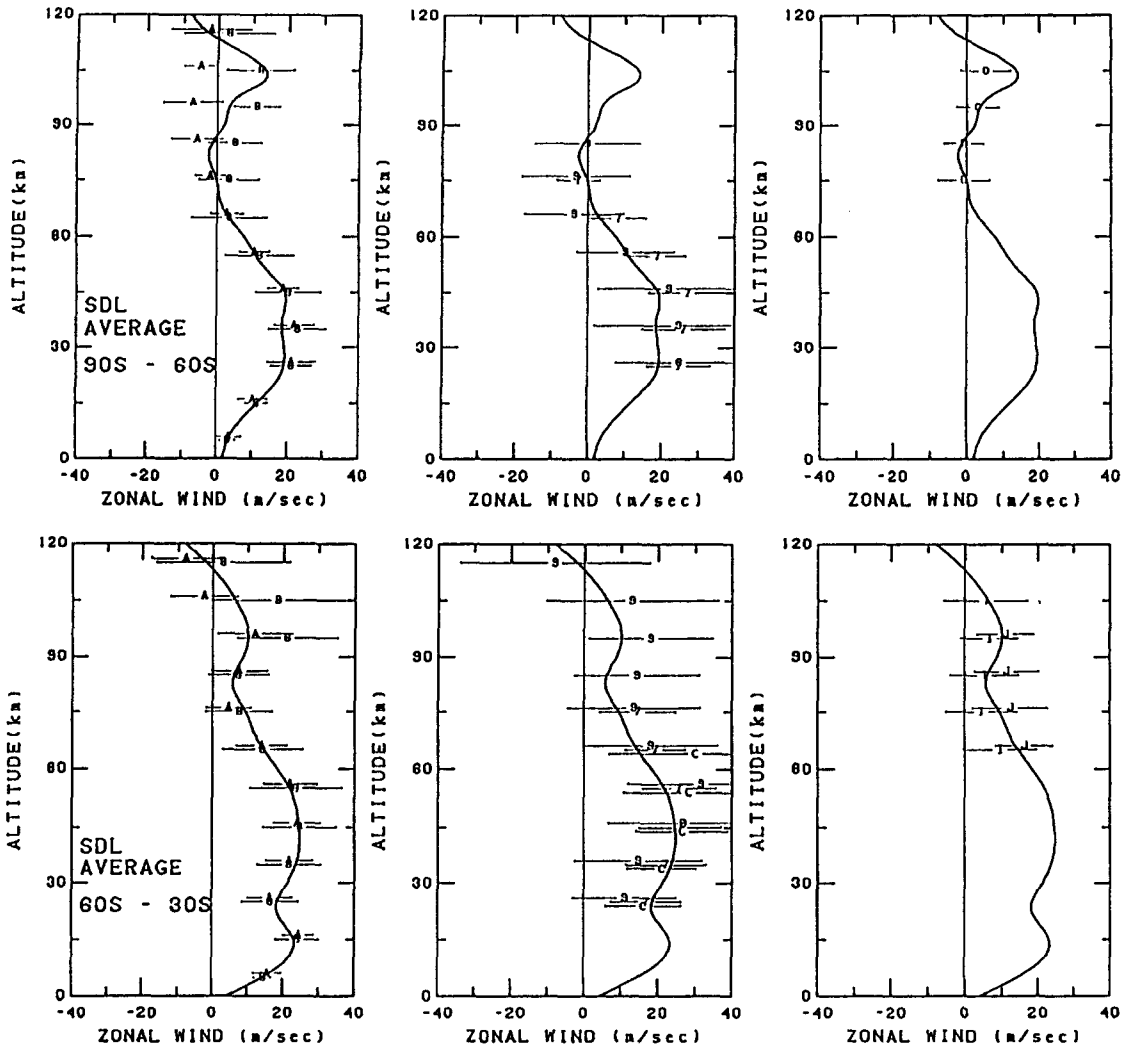

Fig. 2. SDL (seasonal, diurnal, and longitudinal) average zonal wind versus altitude for southern high and middle latitudes. The HWM93 wind (solid line) is shown for mid-range conditions. Plot symbols indicate data source as given in Table 1. Left column of plots contains gradient winds, middle column rocket data, and right column MF/Meteor radar data.

marily stratosphere/mesosphere) and incoherent scatter data (thermosphere); and meteor and MF radars (monthly averages). Examples of the annual average latitude variation are shown in Fig. 5 and annual variation for selected latitude and altitude intervals in Fig. 6.

In the stratosphere the winds are well defined by gradient winds, rocket data, CIRA-72 and CAO-83 (Figs 2–4). The gradient winds are in good agreement with each other except at the equator, thus confirming the representation of temperature and density gradients in MSISE-90. At low latitudes the gradient winds may differ by 5–10 m/s, but neither is systematically in better agreement with the rocket data. Equatorial differences are not surprising given the dependence of the derived zonal wind on the second derivative of pressure as a function of latitude, rather than the first, and the small magnitudes of the terms involved (Fleming and Chandra, 1989). The quasi-biennial variation near the equator will also introduce some scatter. At high latitudes there is a systematic tendency for the rocket data, CIRA-72, and CAO-83 to be higher than the gradient winds in the southern hemisphere, particularly during the equinoxes, and simi-

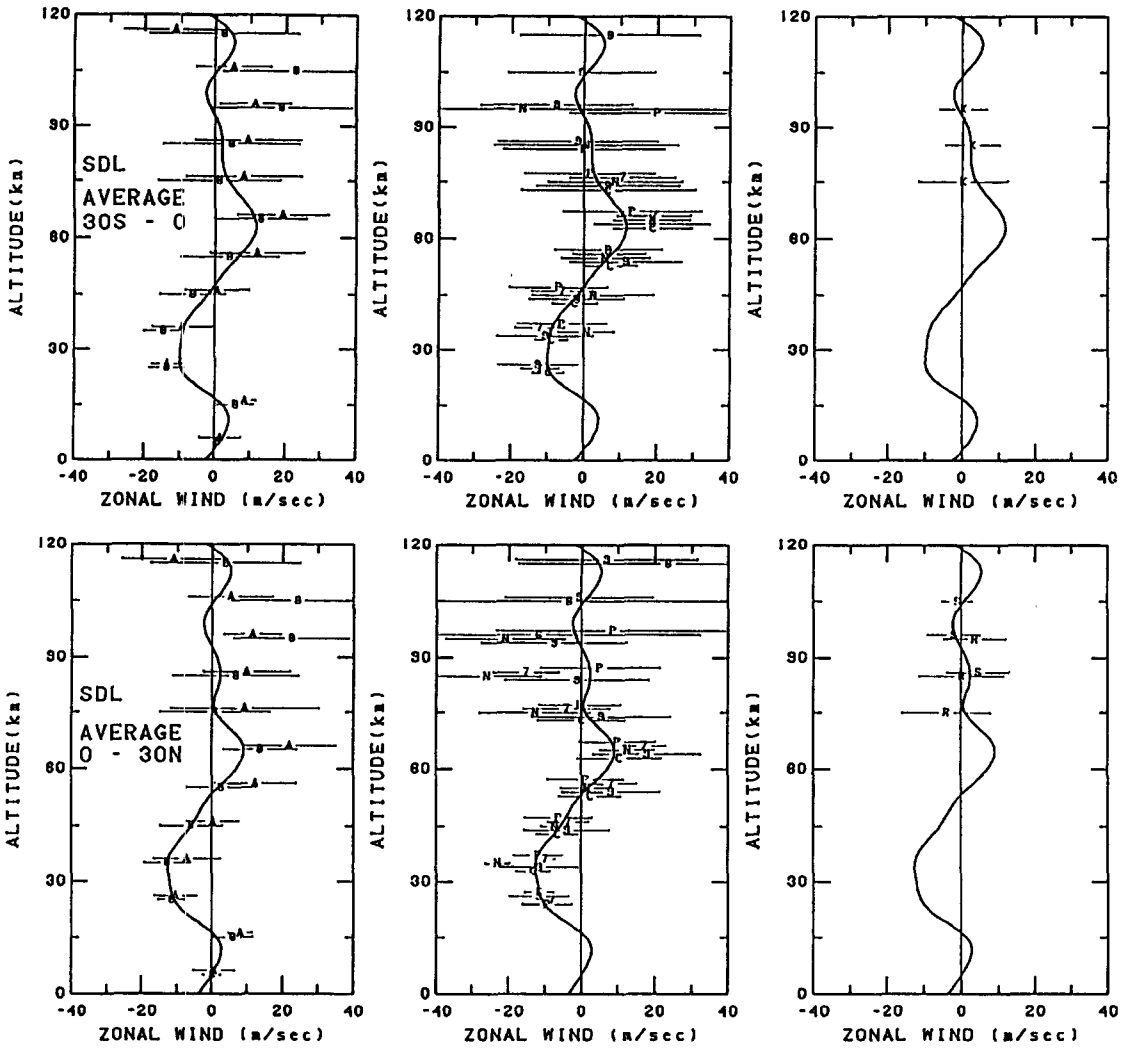

Fig. 3. SDL (seasonal, diurnal and longitudinal) average zonal wind versus altitude for equatorial latitudes. The HWM93 wind (solid line) is shown for mid-range conditions. Plot symbols indicate data source as given in Table 1. Left column of plots contains gradient winds, middle column rocket and IS data, and right column MF/Meteor radar data.

larly lower than the gradient winds in the northern hemisphere.

In the mesosphere the winds are fairly well defined by gradient winds, rocket data, CIRA-72, CAO-83, and Meteor/MF radars, but with increasing scatter and discrepancies toward higher altitudes and at lower latitudes. The Meteor and MF radar values generally differ from the model values by less than 5 m/s. At low latitudes, CIRA-86 is fairly close to the model but MSISE-90 is higher by 10 m/s (Fig. 3). Rocket data show stronger eastward flows than in the model in the lower mesosphere (closer to MSISE-90) and stronger westward flows than in the model in the upper mesosphere (closer to CIRA-86). However, the gradient wind variation as a function of day is qualitatively different from rocket and radar results in the upper mesosphere (Fig. 6). Recently reported equatorial data (Vincent and Lesicar, 1991; Fritts and Isler, 1992) support a strong westward wind in the spring equinox which is quite different from the gradient winds. At mid-latitudes, the rocket data, CIRA-72, and CAO-83 show stronger eastward flow by 5–10 m/s than the gradient or meteor and MF winds (Figs 4 and 5).

The model semiannual amplitude reaches a deeper minimum near 65 km which is more in accord with rocket data than with the amplitude suggested by

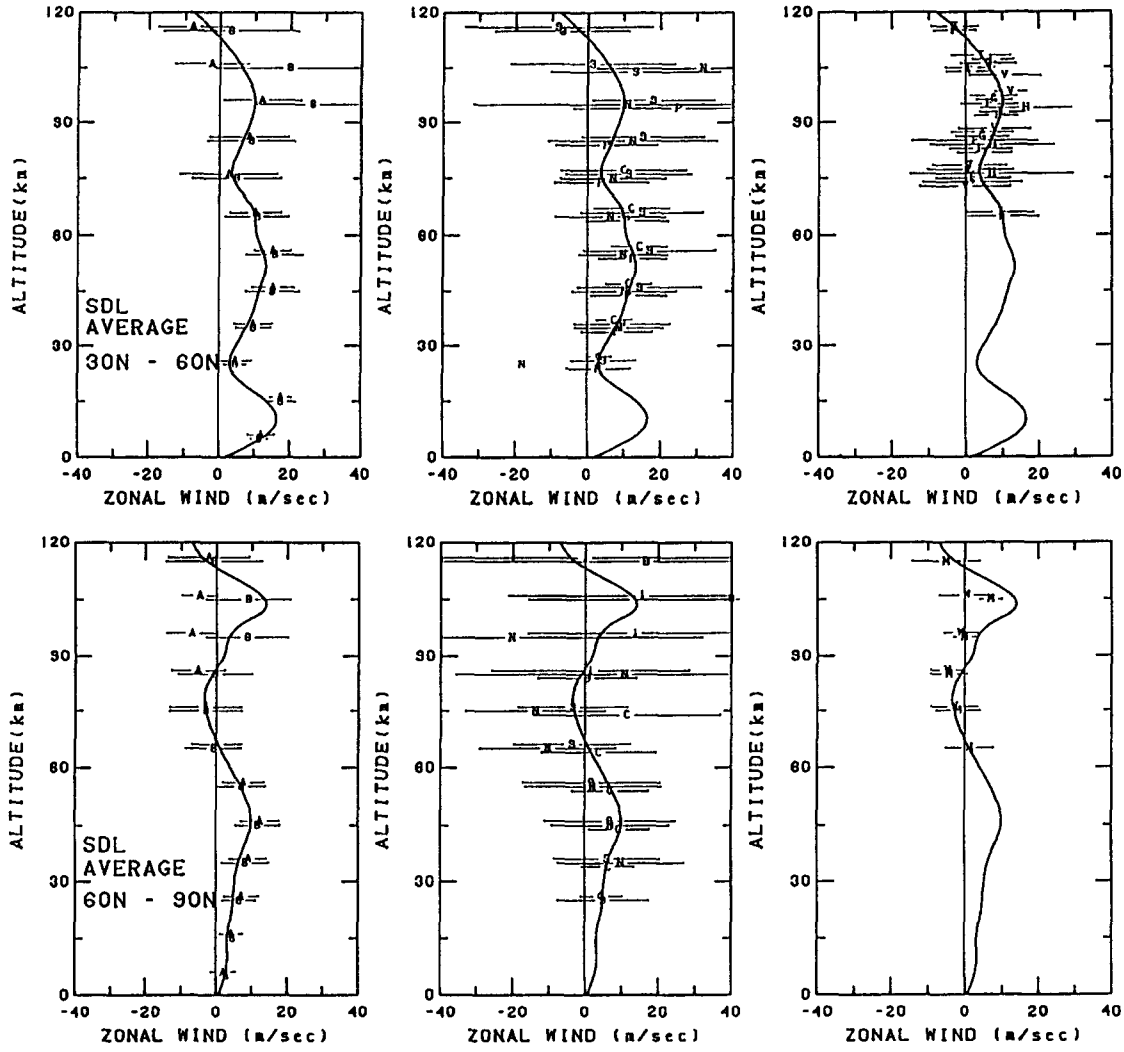

Fig. 4. SDL (seasonal, diurnal and longitudinal) average zonal wind versus altitude for northern high and middle latitudes. The HWM93 wind (solid line) is shown for mid-range conditions. Plot symbols indicate data source as given in Table 1. Left column of plots contains gradient winds, middle column rocket and IS data, and right column MF/Meteor radar data.

gradient winds (Fleming and Chandra, 1989). At northern mid-latitudes near 80 km (Fig. 6), there are small but striking differences in the annual variation observed by different techniques. Meteor radars have a weaker annual variation than either rocket or gradient winds, while the MF radars in this grouping (Saskatoon and Urbana) have an annual variation similar to the gradient winds and larger than the variation described by rocket data. The small average eastward flow in December from the meteor radars leads to an extremely weak (compared to the southern hemisphere winter) eastward mesospheric jet during northern winter in the Miyahara *et al.* (1991) model based only on radar data. Differences in the height of the summer reversal from westward to eastward flow (Manson *et al.*, 1990) also contribute to differences in the annual variation in the 80–90 km region. For example, Saskatoon has a reversal height near 90 km and Atlanta and Kyoto have a reversal height near 80 km. In the lower mesosphere there is considerable separation between CIRA-72 and CAO-83 at high southern latitudes where data have always been sparse.

In the lower thermosphere there is considerable

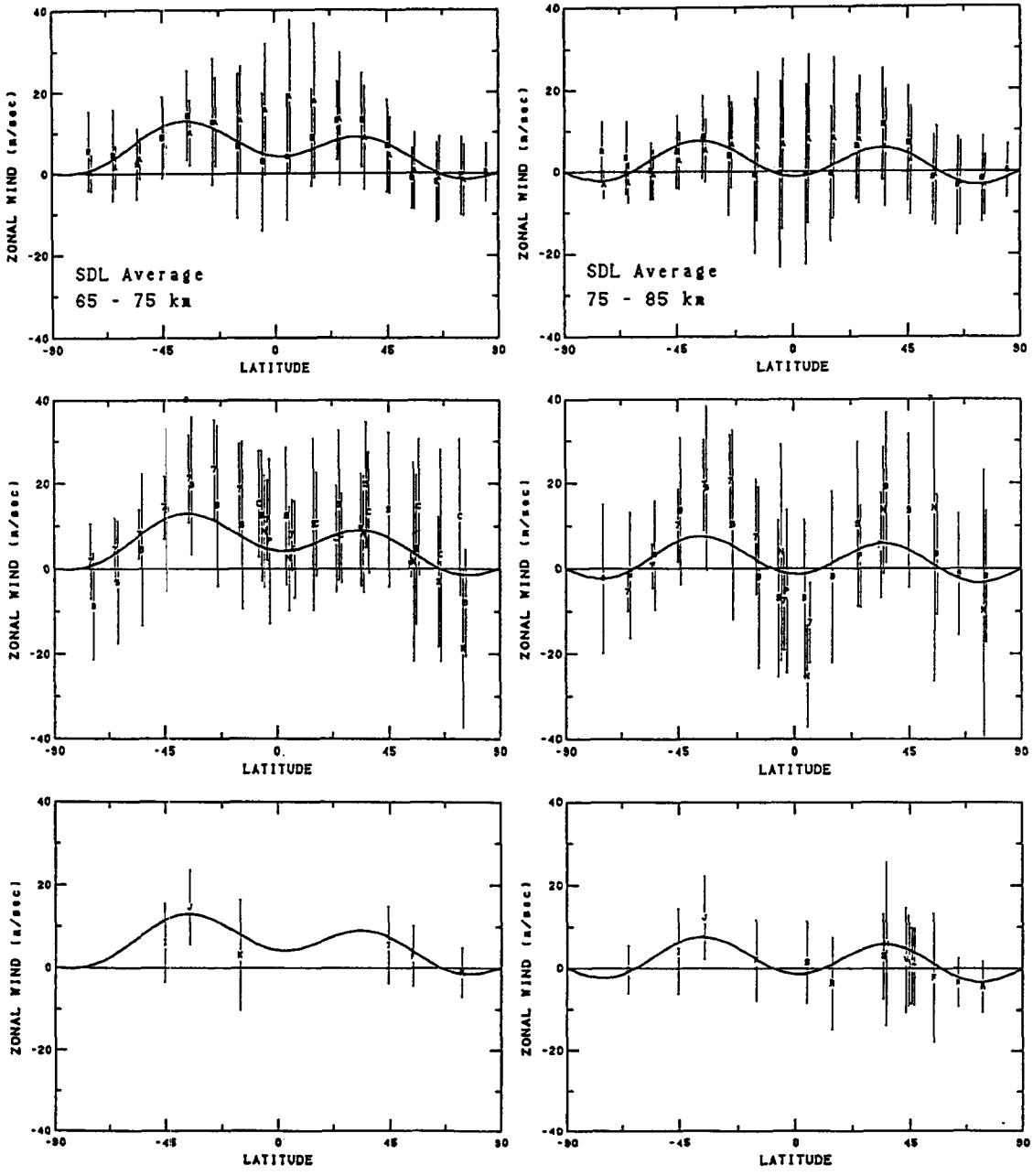

Fig. 5. SDL (seasonal, diurnal and longitudinal) average zonal wind versus latitude for 65 to 75 and 75 to 85 km. The HWM93 wind (solid line) is shown for mid-range conditions. Plot symbols indicate data source as given in Table 1. Top row of plots contains gradient winds, middle row rocket data, and bottom row MF/Meteor radar data.

scatter between data points and sets such that consistency is often poor. The spread between gradient winds is of the order of 10–20 m/s. They follow the model in only a very rough way. The gradient winds are closer to each other and the model during solstices than equinoxes. The Meteor and MF radar data are generally clustered about the model to within 5 m/s on average. At low latitudes, rocket data, CIRA-72, and IS radar values are mostly less than model values while the gradient winds are much above. At high

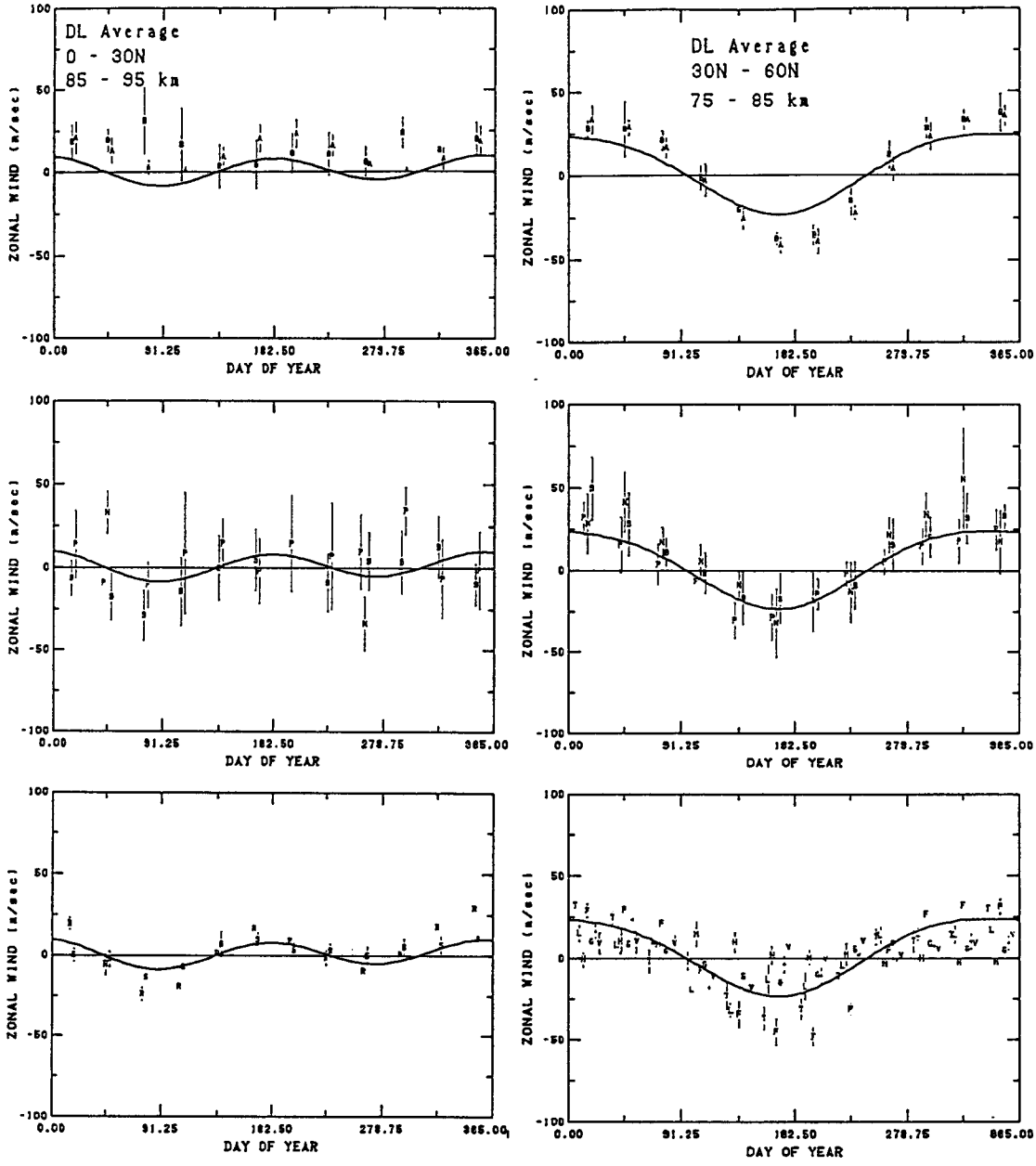

Fig. 6. DL (diurnal and longitudinal) average zonal wind versus day of year for 85 to 95 km at northern low latitudes and 75 to 85 km at northern mid latitudes. The HWM93 wind (solid line) is shown for mid-range conditions. Plot symbols indicate data source as given in Table 1. Top row of plots contains gradient winds, middle row rocket and IS data, and bottom row MF/Meteor radar data.

latitudes, the IS radar values tends to be greater than the model values while the Meteor/MF radar tends to give values less than the model values.

The relatively large eastward winds of CIRA-86 relative to radar data in the lower thermosphere have been discussed by Manson *et al.* (1991). Here the temperature and pressure gradients in the revised MSISE-90 appear to be an improvement over CIRA-86/MSIS-86. The model has weak eastward flow near the equinoxes at mid-latitudes, unlike the strong eastward cell in CIRA-86, but not a complete reversal to the tongue of westward flow seen in radar data. At

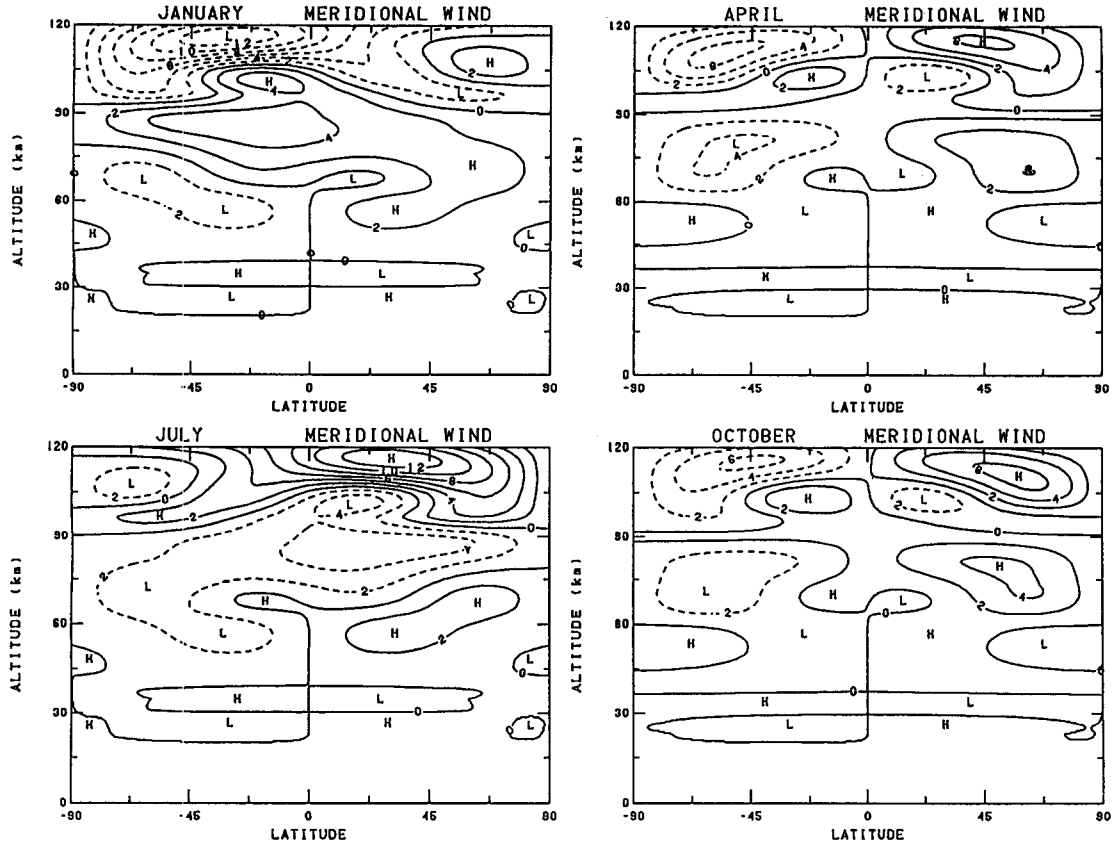

Fig. 7. Contour plots in altitude versus latitude of the DL (diurnal and longitudinal) average meridional wind for four indicated months (mid-month).

low latitudes, CIRA-86 is particularly high relative to rocket, meteor, and MF radar during equinoxes. At high latitudes, incoherent scatter shows larger annual variations in the northern hemisphere (June maximum) than meteor and MF radar or gradient winds. This may be due in part to limited data or biasing by magnetic disturbances when the data yield is best.

Zonal average meridional wind

Example latitudinal cross-sections are shown in Fig. 7 for four different months. The annual variation of the meridional wind has a January northward (southerly) maximum peaking at 4 m/s near the equator in the mesosphere and reversing to a July maximum in the lower thermosphere above 105 km. Only the lowest harmonic in latitude is used below the thermosphere, given the large data scatter, producing meridional winds of the same direction in both hemispheres. The semiannual variation is very small, with an equinox poleward maximum at mid latitudes of 2 m/s in the upper mesosphere and equatorward maximum of 1 m/s in the lower mesosphere. Only the lowest harmonic in latitude is used, providing winds of opposite direction in each hemisphere.

The annual average meridional winds are mostly northward in the northern hemisphere and southward in the southern hemisphere, peaking near 3 m/s in the mesosphere and 6 m/s in the lower thermosphere, with small regions of reverse flow near the mesopause at lower latitudes and the stratopause at high latitudes. The model uses only the two lowest symmetric harmonics so there is no hemispheric difference except in direction of flow.

There is considerable scatter among data points and data sets, as shown for example in Fig. 8. Consistency is often poor, arguing against the use of higher harmonics for a more complicated pattern. However, the rocket data suggest that an alternating pattern in altitude of north/south cells near 75 km in equatorial latitudes is probably stronger than modeled. While the rocket data are fairly consistent in the lower meso-

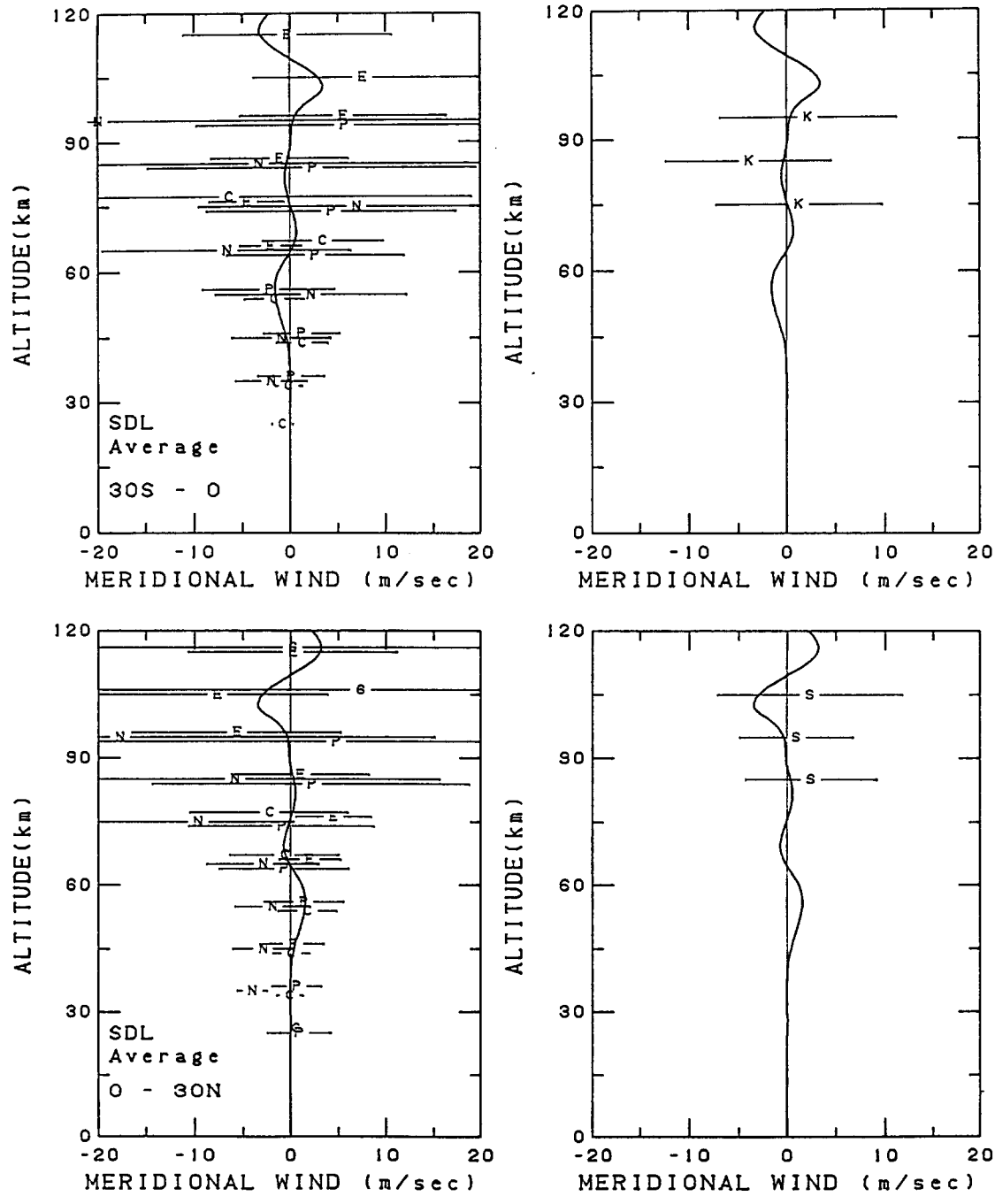

Fig. 8. SDL (seasonal, diurnal and longitudinal) average meridional wind versus altitude for equatorial latitudes. The HWM93 wind (solid line) is shown for mid-range conditions. Plot symbols indicate data source as given in Table 1. Left column of plots contains rocket and IS data data and right column MF/Meteor radar data.

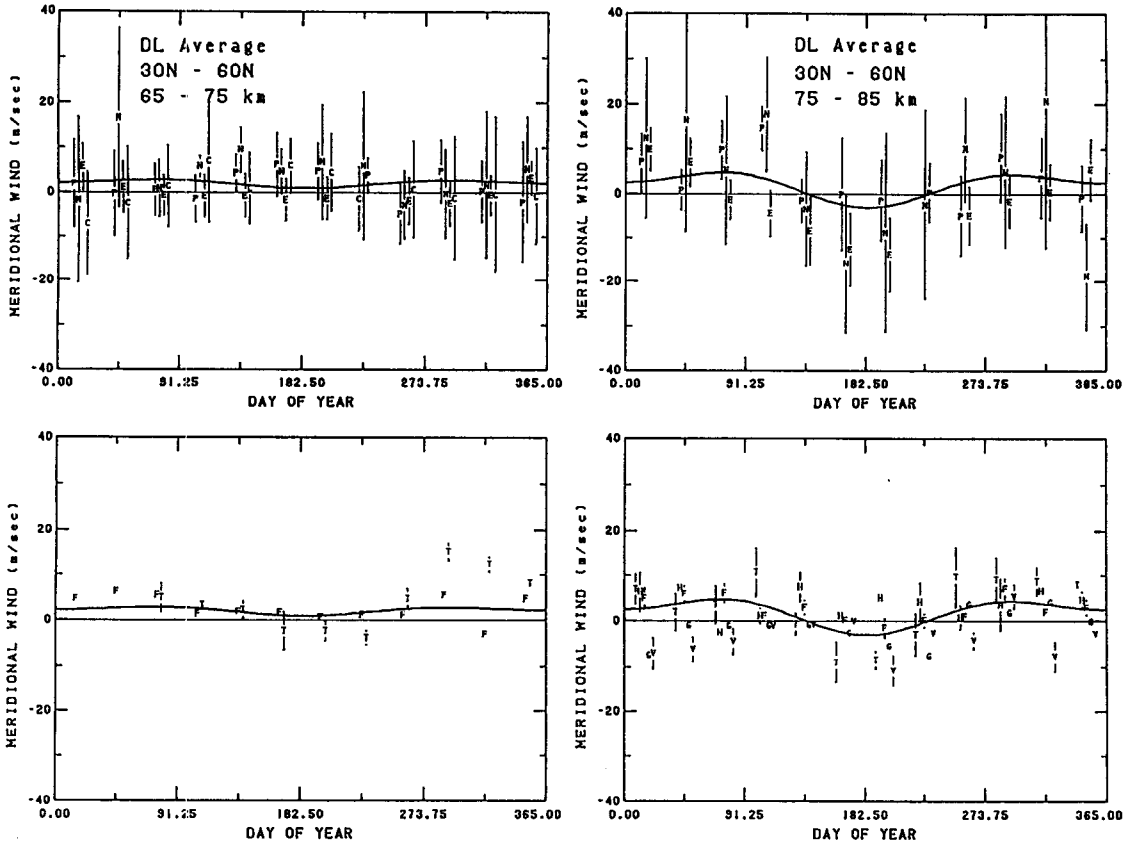

Fig. 9. DL (diurnal, longitudinal) average meridional wind versus day of year for 65 to 75 and 75 to 85 km at northern middle latitudes. The HWM93 wind (solid line) is shown for mid-range conditions. Plot symbols indicate data source as given in Table 1. Top row of plots contains rocket data and bottom row MF/Meteor radar data.

sphere, Groves-69 is inconsistent with meteor and MF radar data in the southern hemisphere. Meteor and MF radar data generally cluster about the model within 5 m/s on average. There are differences of up to 10 m/s among incoherent scatter radar data in the lower thermosphere.

An example of the annual variation is shown in Fig. 9. There is considerable scatter among data points and data sets; however, overall model trends are clearly present in the data, even if details are not particularly robust. While fluctuations in meridional and zonal wind measurements are similar, the desired average signal is much smaller for the meridional wind relative to the fluctuations; thus incomplete coverage in the rocket and incoherent scatter data is more noticeable. Seasonal patterns are often similar to Groves (1969) but often of lesser magnitude. Latitudinal patterns are also similar to those of Miyahara *et al.* (1991), based exclusively on radar data, although less detailed. In particular, our analysis did not find a region of winter to summer flow near 80 km at equatorial latitudes (embedded in the more typical summer to winter flow). The characteristics of the summer to winter flow as found in radar data and the relation to measured momentum deposition by gravity waves has been discussed by Manson *et al.* (1991). The reversal to a winter to summer flow in the lower thermosphere is clearly present in the MF/Meteor radar data, as it was in the incoherent scatter data (Hedin *et al.*, 1991), but again with station to station differences in reversal height, as for the zonal wind.

Longitude variations

Stationary wave 1 (first harmonic in longitude) variations are represented by an average variation with latitude and an annual and semiannual variation about the average. The zonal variations peak in the upper stratosphere at northern winter mid-latitudes, with an amplitude of 30 m/s (zonal), and again at the pole with an amplitude of 35 m/s (zonal and meridi-

onal). Meridional wind variations peak at the pole with the same amplitude. Southern hemisphere amplitudes are less than 10 m/s. Longitude variations related to planetary waves are not carried above 90 km for lack of defining data (but longitude variations are present in the thermosphere above 130 km because of physical processes tied to the magnetic field geometry) or below 15 km (limited by the CIRA tabulations).

The longitude variations are derived almost entirely from gradient wind data (Fleming *et al.*, 1990). Winds from MSISE-90 are generally similar with two significant exceptions. Near the poles, where there was difficulty in performing the numerical differentiation from the tabulated satellite data, the winds from CIRA do not properly approach a common magnitude. Near the equator where the wind depends on a second derivative of pressure, the MSISE-90 based winds suffer from a lack of latitude resolution. The month to month variability is remarkably well represented by a sum of annual and semiannual variations in the longitudinal harmonic coefficients. Other data are nominally consistent, but are insufficient in longitude coverage to define the variation. In particular, the CIRA-72 tables, separated by American and European longitudes, are reasonably consistent with the satellite data. See Hedin *et al.* (1993a) for model and comparison plots.

Second harmonic (wave 2) variations are present (Barnett and Labitzke, 1990; Fleming *et al.*, 1990) in the stratosphere and mesosphere but, unlike the wave 1 variations, their month to month variability is more random and not as usefully represented in terms of a mean, with annual and semiannual variations, and is thus not included in this model.

Diurnal variations

Diurnal variations are represented by an annual average and annual variation about the average. Amplitudes are weak in the stratosphere and lower mesosphere (a few meters per second), but reach a peak of tens of meters per second at low- to mid-latitudes in the upper mesosphere and lower thermosphere, and are generally dominant over the semidiurnal tide in the upper mesosphere. At high latitudes, amplitudes peak even more strongly between 110 and 120 km. The accuracy of detailed latitude patterns near the equator in the mesosphere and in southern latitudes in the lower thermosphere is uncertain because of the lack of data gathering stations. Aspects of the tidal climatology have been discussed by Avery *et al.* (1989) and Manson *et al.* (1989).

The annual variation of the diurnal amplitudes and phases of the meridional and zonal wind is illustrated for two latitudes in Figs 10 and 11, corresponding to the locations of the Saskatoon and Christchurch radars. In the upper mesosphere, the meridional amplitude tends to maximize in the summer. The zonal seasonal variation is weaker and less clear. Some stations also had significant semiannual variations but consistency with other stations was not always good.

Examples of model winds and comparisons with data are shown in Figs 12 and 13. There are two plots separating data into two groups: rocket data (stratosphere and mesosphere) and incoherent scatter data (thermosphere), and meteor and MF radars (mesosphere and lower thermosphere). Large standard deviations for the radars are partly the result of interannual and month to month tidal variability. Individual data amplitudes will frequently tend to be larger than model amplitudes because varying or inconsistent phases between data points produce a cancellation effect during generation of the model. The model is based on Fourier components; data to model differences were calculated with the Fourier components and then the amplitudes and phases reconstructed. Other comparison plots were presented by Hedin *et al.* (1993b). Climatological aspects of the tides as measured by radar were discussed by Avery *et al.* (1989), Manson *et al.* (1989) and Vincent *et al.* (1989).

At mid-latitudes, for example (Fig. 13), the values derived from several radar stations were somewhat diverse in measured phases and helped reduce the model amplitude relative to the measured zonal amplitudes. At high latitudes the broad seasonal trends in amplitude and phase were captured fairly well, except for the meridional phase at Mawson. Hemispherical asymmetries apparently have a more complicated latitude dependence than assumed here. A strong annual variation in meridional amplitude at Christmas Island, without accompanying phase changes or zonal changes, could not be captured by the limited harmonic model. The model does not have the strong asymmetry between Adelaide and Kyoto described by Vincent *et al.* (1989). However, there are clearly differences between Adelaide and relatively nearby Christchurch, while Kyoto in general has lower amplitudes than nearby (in latitude) northern hemisphere stations (and uses a different measurement technique from that used at the southern hemisphere stations). It is not clear to what degree differences with the model reflect the low latitude resolution of the model, differences in measurement technique, peculiarities of individual sites or, possibly, inter-annual variability.

In the upper stratosphere and lower mesosphere, tides are determined only by rocketsonde data which

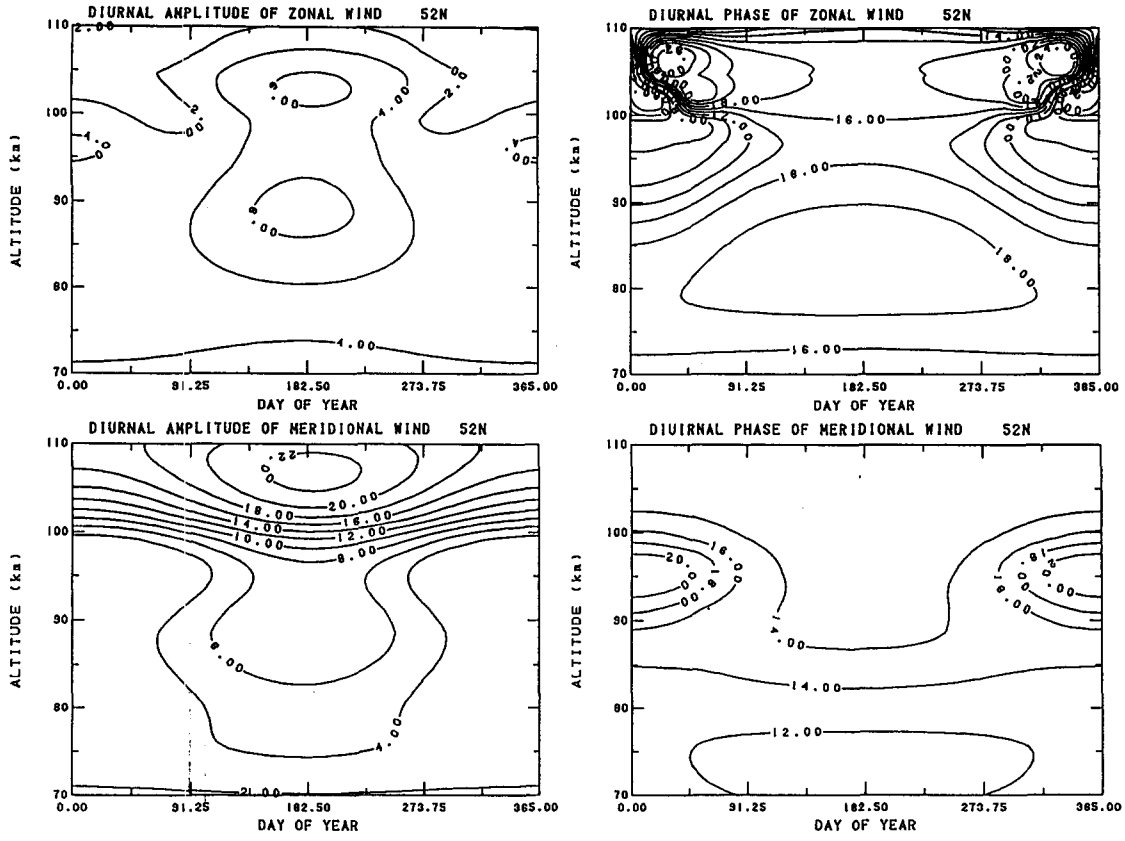

Fig. 10. Contour plots in altitude versus day of year of the diurnal amplitude and phase (dashed negative) of the zonal and meridional wind at 52°N latitude.

are sparse in the southern hemisphere and generally have incomplete local time coverage for individual months. Thus, the model does not include interhemispheric differences or seasonal variations below 75 km. While the scatter of the original measurements can be considerable (particularly at high latitudes) and measurements at different local times are usually from different days, diurnal variations are clearly present, with rapid phase changes with height near the equator and little phase change with height below 100 km at higher latitudes. Amplitudes are not very reliable at high latitudes because of the large scatter in the original point measurements. The eastward wind maximizes about six hours later than the northward wind in the northern hemisphere and six hours earlier than the northward wind in the southern hemisphere. These features were previously seen in the analysis of earlier data (Reed *et al.*, 1969; Groves, 1980) and are broadly consistent with theory (Forbes, 1982), although theory tends to predict a higher contribution of propagating modes at mid latitudes, and thus more rapid phase changes with altitude, than observed.

Rocket data become increasingly scattered in the upper mesosphere so that amplitudes are suspect, but phases generally blend smoothly with MF/Meteor radar data at their lower altitude limit. Model phases agree quite well with MF/Meteor data. The lowest latitude data (Townsville (20°S), Christmas Island (2°N), and Punta Borinquen (18°N)) suggest higher diurnal amplitudes in the upper mesosphere, but these data are from very limited time series. With Kyoto (35°N) amplitudes generally being on the small side and those at Adelaide (35°S) on the high side, it is difficult to fit all these stations without increasing the harmonic order considerably and introducing complex latitude and interhemispheric variations which may not be justified. All comparisons must be considered against the background of significant variability in both the diurnal and semidiurnal tides (e.g. Fritts and Isler, 1992) and the fact that the stations are not equivalent in their seasonal coverage or years of measurement.

In the lower thermosphere at high latitudes, the rapid change in diurnal phase above 100 km with

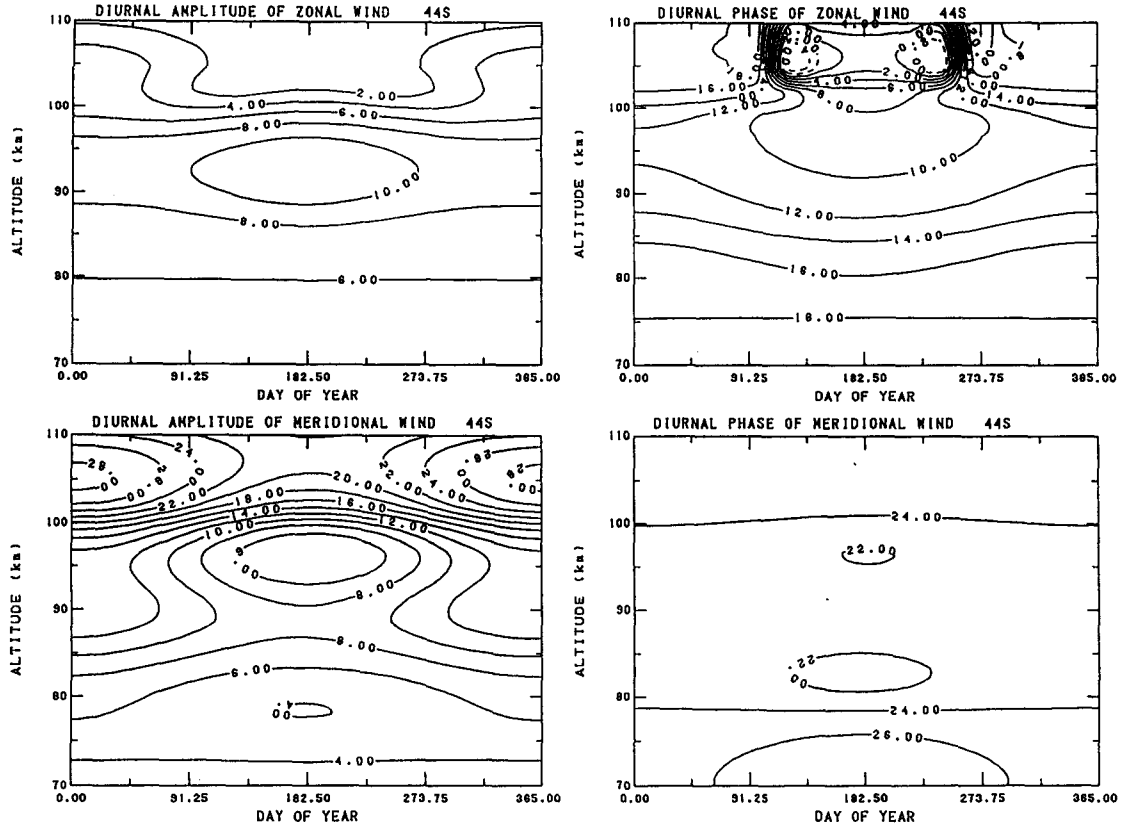

Fig. 11. Contour plots in altitude versus day of year of the diurnal amplitude and phase (dashed negative) of the zonal and meridional wind at 44°S latitude.

increasing amplitudes into the thermosphere is reflected in both MF/Meteor data and IS data. However, at mid- to low-latitudes the lack of full daytime coverage by IS plus considerable differences between MF/Meteor radar stations makes the transition of the diurnal tide into the thermosphere poorly defined.

Semidiurnal variations

Semidiurnal variations are represented by an annual average, with annual and semiannual variation about the average. Amplitudes are weak in the stratosphere and lower mesosphere (a few meters per second). However, amplitudes increase strongly to a peak of 40–60 m/s, and are dominant over the diurnal variation, in the lower thermosphere. The accuracy of the detailed latitude patterns near the equator in the mesosphere and in southern latitudes in the lower thermosphere is uncertain because of the lack of data gathering stations.

The annual variation of the semidiurnal amplitudes and phases of the meridional and zonal wind is illustrated for two latitudes in Figs 14 and 15. Semiannual trends in amplitude are quite pronounced, particularly in the southern hemisphere. However, vertical wavelengths in the mesosphere are shorter in winter than in summer, as discussed by Manson *et al.* (1989).

Model and data comparison plots similar to those for diurnal variations are shown in Figs 16 and 17. As with the diurnal component, the significant variability of tides must be kept in mind. These figures also show the corresponding model prediction from the Forbes and Vial (1989) model (FV89).

In the upper stratosphere and lower mesosphere the same data limitations apply as for diurnal variations. The model does not include interhemispheric differences or seasonal variations below 75 km. Semidiurnal variations are clearly present at low- to mid-latitudes with systematic phase variations with height. Amplitudes are again not very reliable at high latitudes because of the large scatter in the point measurements.

Rocket data become increasingly scattered in the upper mesosphere so that amplitudes are suspect, but

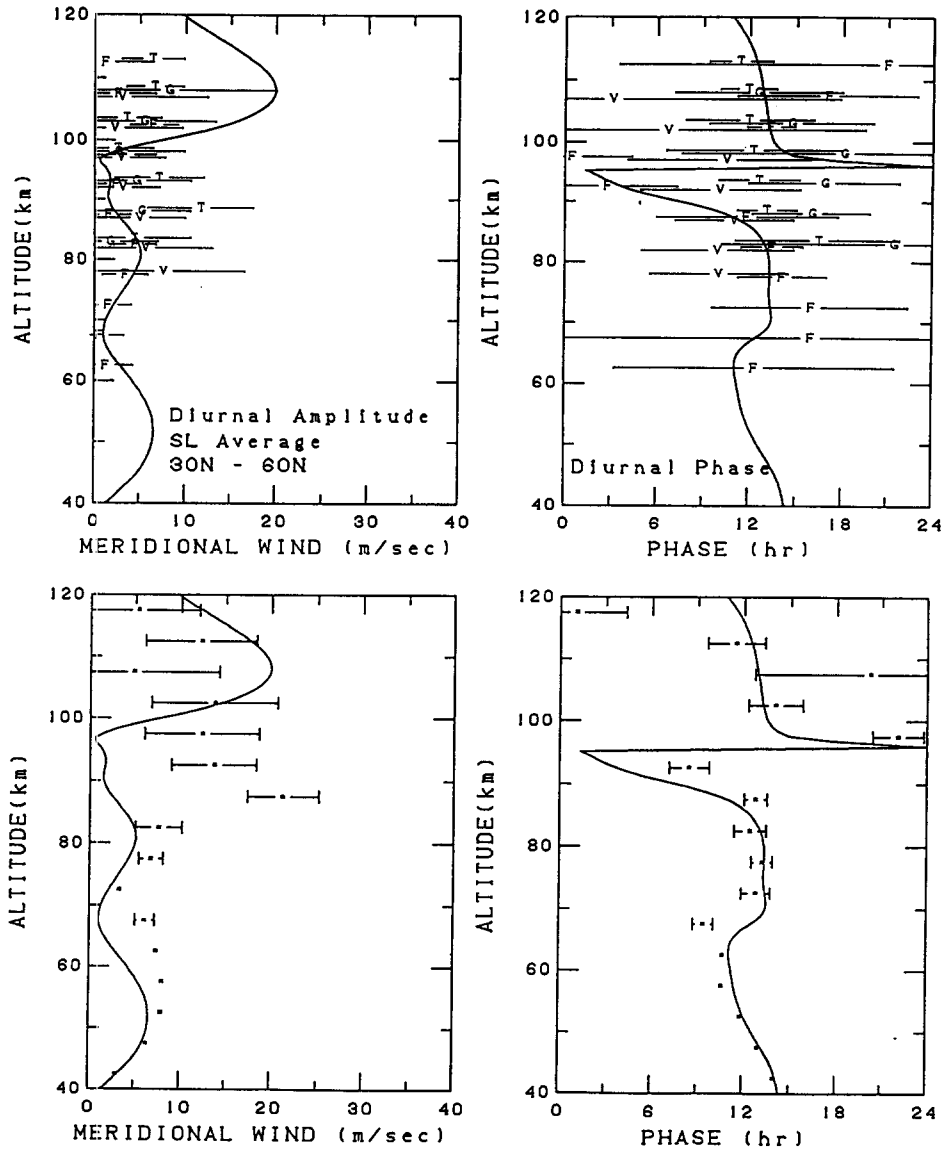

Fig. 12. SL (seasonal and longitudinal) average diurnal meridional wind amplitude and phase versus altitude for northern middle latitudes. The HWM93 wind (solid line) is shown for mid-range conditions. Top row of plots contains MF/Meteor radar data with plot symbols indicated in Table 1. Bottom row contains rocketsonde and IS radar data combined (*).

phases generally blend smoothly with MF/Meteor radar data at their lower altitude limit. Model phases agree quite well with MF/Meteor data, except for the Townsville zonal phase, which differs significantly from its northern hemisphere counterparts.

Semidiurnal amplitudes increase strongly into the lower thermosphere according to IS data, but not as strongly in MF/Meteor radar data (Fig. 16). However, MF radar data above 100 km are subject to group retardation effects. Amplitudes from the Forbes and Vial (1989) model are generally the same order of magnitude as from the data and HWM93 model, with similar phase patterns overall.

Data comparison plots for annual variations are shown in Fig. 17, including the Forbes and Vial (1989) model, FV89. The annual trends in amplitude and phase at middle to high latitudes were captured fairly well. Phases have a more noticeable annual variation

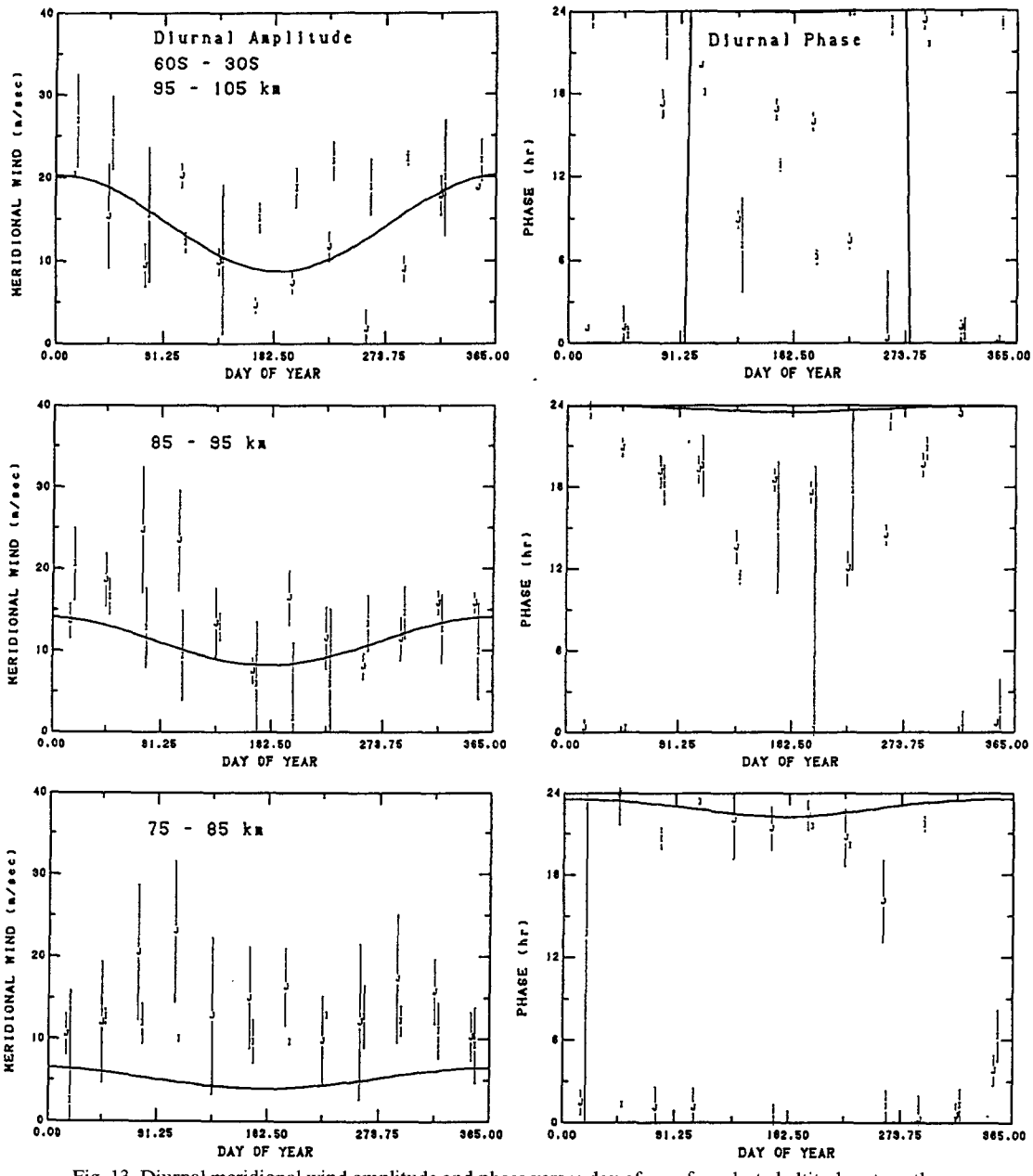

Fig. 13. Diurnal meridional wind amplitude and phase versus day of year for selected altitudes at southern middle latitudes. The HWM93 model (solid line) is shown for mid-range conditions. Plot symbols indicate source as given in Table 1.

than amplitudes, while amplitudes have a more semi-annual character in the southern hemisphere with equinoctial maxima. The FV89 model is generally similar but with a larger seasonal variation in the lower thermosphere. The greater diversity of measurement phases at mid-latitudes leads to modeled amplitudes smaller than given by the measurements. Neither HWM93 nor FV89 does particularly well with the Christchurch and Adelaide meridional phases. Christchurch amplitudes are generally higher than for the model and data from Adelaide, but data over several years reported by Fraser (1990) indicate that the data used here from 1979 may be unusually high.

At equatorial latitudes, the trends at Christmas

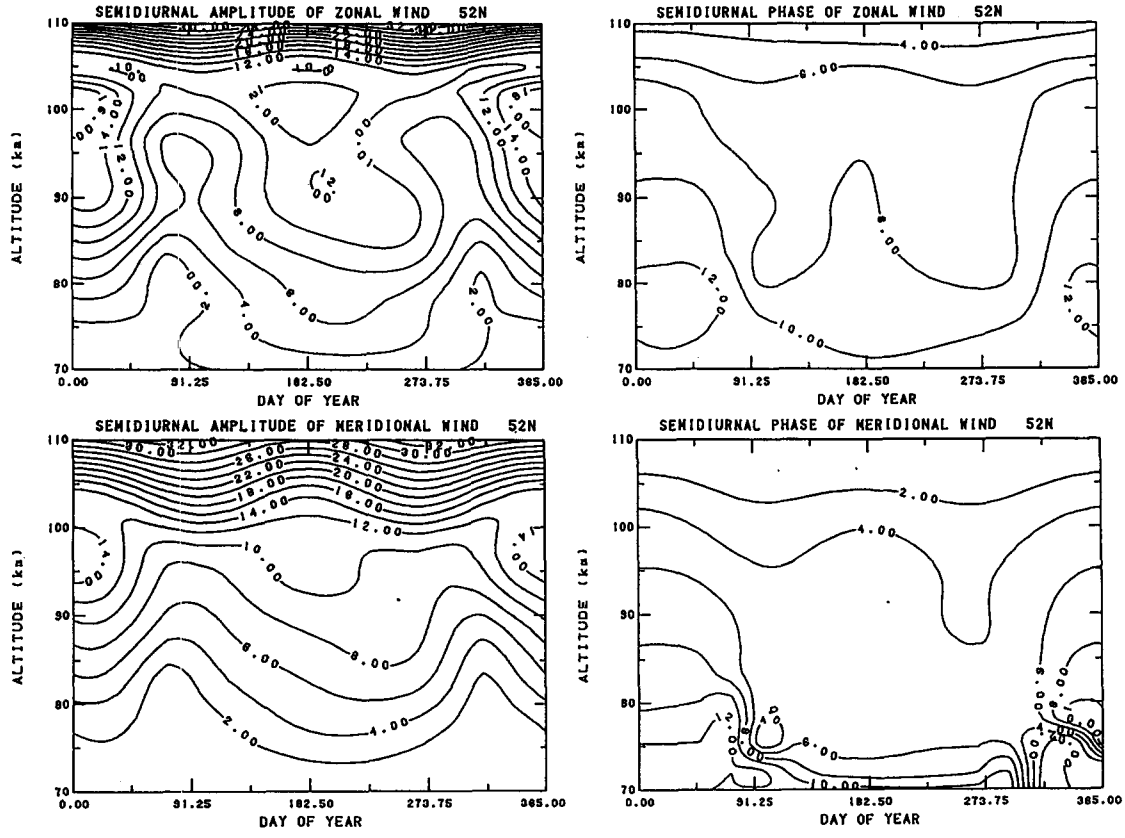

Fig. 14. Contour plots in altitude versus day of year of the semidiurnal amplitude and phase (dashed negative) of the zonal and meridional wind at 52°N latitude.

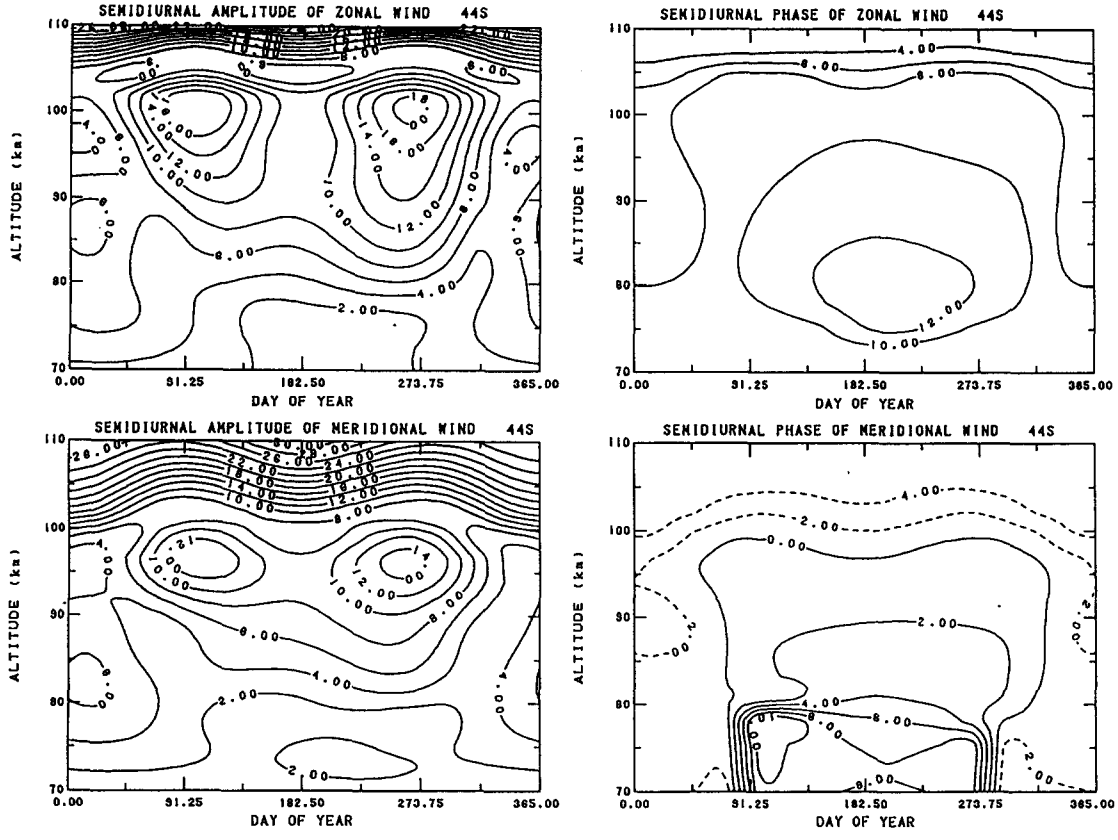

Fig. 15. Contour plots in altitude versus day of year of the semidiurnal amplitude and phase (dashed negative) of the zonal and meridional wind at 44°S latitude.

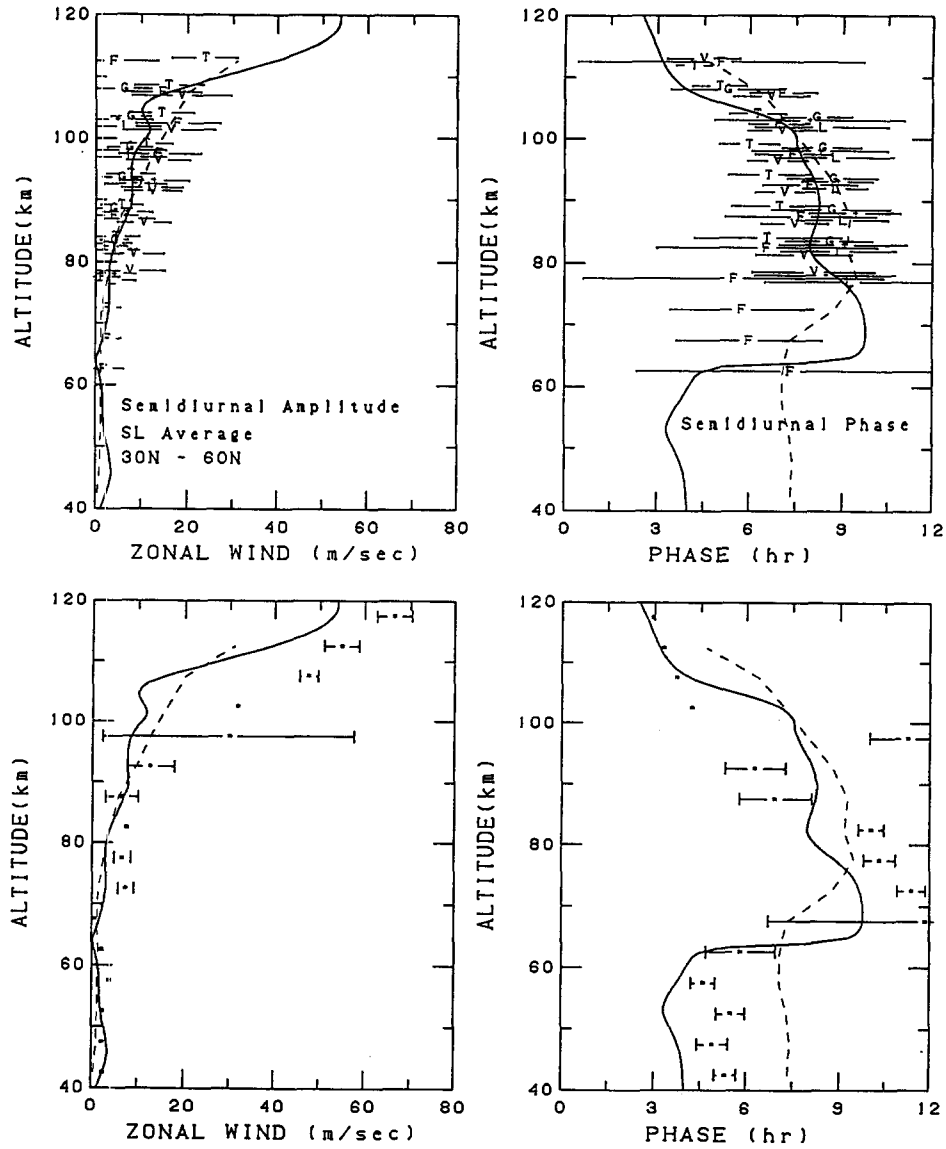

Fig. 16. SL (seasonal and longitudinal) average semidiurnal zonal wind amplitude and phase versus latitude for northern middle latitudes. The HWM93 wind (solid line) and FV89 (dashed) shown for mid-range conditions. Top row of plots contains MF/Meteor radar data with symbols indicated in Table 1. Bottom row contains rocketsonde and IS radar data combined (*).

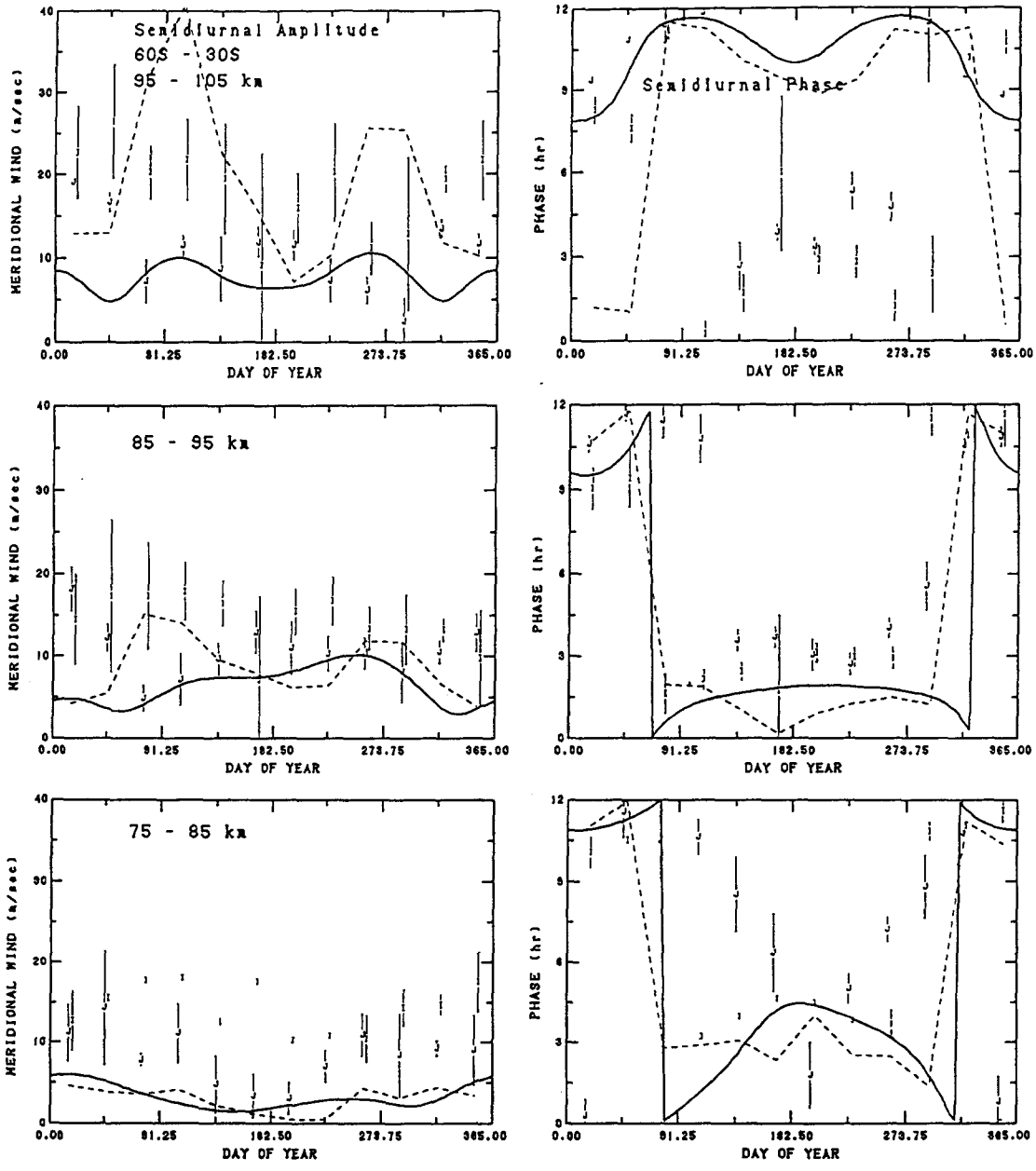

Fig. 17. Semidiurnal meridional wind amplitude and phase versus day of year for selected altitudes at southern middle latitudes. The HWM93 model (solid line) and FV89 (dashed) shown for mid-range conditions. Plot symbols indicate source as given in Table 1.

Island were captured better than for the diurnal tide. The FV89 zonal phase appears to be systematically offset from HWM93 at low latitudes.

SUMMARY

Reference winds from CIRA-86 combined with rocket soundings, incoherent scatter, MF radar, meteor radar, and older reference tabulations have been used to extend the HWM90 spherical harmonic wind model into the lower atmosphere, providing a unified description of zonal and meridional prevailing winds from the surface to the exosphere and tidal components from the upper stratosphere. While month to month details cannot be completely represented, mesospheric data are fitted to an overall rms

error of approximately 15 m/s and considerably better in the stratosphere. Comparison with rocket and radar data indicates that the model represents current knowledge of climatology reasonably well.

Acknowledgements—A FORTRAN subroutine is available from the National Space Science Data Center Request Coordinator Office (NSSDC/code 933.8, Goddard Space Flight Center, Greenbelt, MD 20771; Tel. (301)286-6695; Span NCF:REQUEST).

REFERENCES

Angell J. K. and Korshover J. 1970 Quasi-bienniel, annual, and semi-annual zonal wind and temperature harmonic amplitudes and phases in the stratosphere and lower mesosphere of the northern hemisphere, *J. geophys. Res.* **75,** 543–550.

Avery S. K., Riddle A. C. and Balsley B. B. 1983 The Poker Flat, Alaska, MST radar as a meteor radar, *Radio Sci.*, **18,** 1021–1027.

Avery S. K., Vincent R. A., Phillips A., Manson A. H. and Fraser G. J. 1989 High-latitude tidal behavior in the mesosphere and lower thermosphere. *J. atmos. terr. Phys.* **51,** 595–608.

Avery S. K., Avery J. P., Valentic T. A., Palo S. E., Leary M. J. and Obert R. L. 1990 A new meteor echo detection and collection system: Christmas Island mesospheric wind measurements, *Radio Sci.* **25,** 657–669.

Barnett J. J. and Corney M. 1985 Middle atmosphere reference model from satellite data, *Handbook for MAP*, **16,** edited by K. Labitzke, J. J. Barnett, and B. Edwards, pp. 47–85, SCOSTEP, Urbana, Ill.

Barnett J. J. and Labitzke K. 1990 Climatological distribution of planetary waves in the middle atmosphere, *Adv. Space Res.* **10**(12), 63–91.

Belmont A. D. 1985 Comparisons of time-periodic variations in temperature and wind from meteorological rockets and satellites, *Adv. Space Res.* **5**(7), 115–123.

Bernard R. 1974 Tides in the E-region observed by incoherent scatter over Saint Santin, *J. atmos. terr. Phys.* **36,** 1105–1120.

Bernard R., Fellous J. L., Massebeuf M. and Glass M. 1981 Simultaneous meteor radar observations at Monpazier (France, 44°N) and Punta Borinquen (Puerto-Rico, 18°N). I-Latitudinal variations of atmospheric tides, *J. atmos. terr. Phys.* **43,** 525–533.

Clark R. R. 1983 Upper atmosphere wind observations of waves and tides with the UNH Meteor Radar System at Durham 43°N (1977, 1978 and 1979), *J. atmos. terr. Phys.* **45,** 621–627.

Fleming E. L. and Chandra S. 1989 Equatorial zonal wind in the middle atmosphere derived from geopotential height and temperature data, *J. Atmos. Sci.* **46,** 860–866.

Fleming E. L., Chandra, S. Barnett J. J. and Corney M. 1990 Zonal mean temperature, pressure, zonal wind and geopotential height as functions of latitude *Adv. Space Res.* **10**(12), 11–59.

Forbes J. M. 1982 Atmospheric tides 1. Model description and results for the solar diurnal component, *J. geophys. Res.* **87,** 5222–5240.

Forbes J. M. and Vial F. 1989 Monthly simulations of the solar semidiurnal tide in the mesosphere and lower thermosphere, *J. atmos. terr. Phys.* **51,** 649–661.

Franke S. J. and Thorsen D. 1993 Mean winds and tides in the upper middle atmosphere at Urbana (40°N, 88°W) during 1991–1992, *J. geophys. Res.* **98,** 18607–18615.

Fraser G. J. 1990 Long-term variations in mid-latitude southern hemisphere mesospheric winds, *Adv. Space Res.* **10**(10), 247–250.

Fritts D. C. and Isler J. R. 1992 First observations of mesospheric dynamics with a partial reflection radar in Hawaii (22°N, 160°W), *Geophys. Res. Lett.* **19,** 409–412.

Groves G. V. 1969 Wind models from 60 to 130 km altitude for different months and latitudes, *J. Brit. Interplanet. Soc.* **22,** 285–307.

Groves G. V.	1972a	Atmospheric structure and its variations in the region from 25 to 120 km, in *CIRA* 1972, pp. 33–224, Akademie-Verlag, Berlin.
Groves G. V.	1972b	Annual and semi-annual zonal wind components and corresponding temperature and density variations, 60–130 km, *Planet. Space Sci.* **20,** 2099–2112.
Groves G. V.	1980	Seasonal and diurnal variations of middle atmosphere winds, *Phil. Trans. R. Soc. Lond.* **A296,** 19–40.
Harper R. M.	1977	Tidal winds in the 100- to 200-km region at Arecibo, *J. geophys. Res.* **82,** 3243–3250.
Harper R. M., Wand R. H., Zamlutti C. J. and Farley D. T.	1976	E region ion drifts and winds from incoherent scatter measurements at Arecibo, *J. geophys. Res.* **81,** 25–37.
Hedin A. E.	1983	A revised thermospheric model based on mass spectrometer and incoherent scatter data: MSIS-83, *J. geophys. Res.* **88,** 10,170–10,188.
Hedin A. E.	1987	MSIS-86 thermospheric model *J. geophys. Res.* **92,** 4649–4662.
Hedin A. E.	1988	The atmospheric model in the region 90 to 2000 km *Adv. Space Res.* **8**(5), 9–25.
Hedin A. E.	1991	Extension of the MSIS thermosphere model into the middle and lower atmosphere, *J. geophys. Res.* **96,** 1159–1172.
Hedin A. E., Spencer N. W. and Killeen T. L.	1988	Empirical global model of upper thermosphere winds based on Atmosphere and Dynamics Explorer satellite data *J. geophys. Res.* **93,** 9959–9989.
Hedin A. E., Biondi M. A., Burnside R. G., Hernandez G., Johnson R. M., Killeen T. L., Mazaudier C., Meriwether J. W., Salah J. E., Sica R. J., Smith R. W., Spencer N. W., Wickwar V. B. and Virdi T. S.	1991	Revised global model of thermosphere winds using satellite and ground-based observations, *J. geophys. Res.* **96,** 7657–7688.
Johnson R. M., Wickwar V. B., Roble R. G. and Luhmann J. G.	1987	Lower-thermosphere winds at high latitude: Chatanika radar observations, *Ann. Geophys.* **5A,** 383–404.
Koshelkov Y. P.	1983	Proposal for a reference model of the middle atmosphere of the southern hemisphere *Adv. Space Res.* **3**(1), 3–16.
Koshelkov Y. P.	1990	Southern hemisphere reference middle atmosphere *Adv. Space Res.* **10**(12), 245–263.
MacLeod R. and Vincent R. A.	1985	Observations of winds in the Antarctic summer mesosphere using the spaced antenna technique, *J. atmos. terr. Phys.* **47,** 567–574.
Manson A. H. and Meek C. E.	1991	Climatologies of mean winds and tides observed by medium frequency radars at Tromso (70°N) and Saskatoon (52°N) during 1987–1989, *Can. J. Phys.* **69,** 966–975.
Manson A. H., Meek C. E. and Gregory J. B.	1981	Winds and waves (10 min-30 days) in the mesosphere and lower thermosphere at Saskatoon (52°N, 107°W, L = 4.3) during the year, October 1979 to July 1980, *J. geophys. Res.* **86,** 9615.
Manson A. H., Meek C. E., Massebeuf M., Fellous J. L., Elford W. G., Vincent R. A., Craig R. L., Roper R. G., Avery S., Balsley B. B., Fraser G. J., Smith M. J., Clark R. R., Kato S., Tsuda T. and Ebel E.	1985	Mean winds of the upper middle atmosphere (60–110 km): A global distribution from radar systems (M.F., Meteor, VHF) *Handbook for Map,* **16,** Eds. K. Labitzke, J. J. Barnett, and B. Edwards, Urbana IL, 239–268.
Manson A. H., Meek C. E., Massebeuf M., Fellous J. L., Elford W. G., Vincent R. A., Craig R. L., Phillips A., Roper R. G., Fraser G. J., Smith M. J., Avery S., Balsley B. B., Clark R. R., Kato S., Tsuda T., Schminder R. and Kuerschner D.	1990	Description and presentation of reference atmosphere radar winds (80–110 km) *Adv. Space Res.* **10**(12), 267–315.
Manson A. H., Meek C. E., Fleming E., Chandra S., Vincent R. A., Phillips A., Avery S. K., Fraser G. J., Smith M. J., Fellous J. L. and Massebeuf M.	1991	Comparisons between satellite-derived gradient winds and radar-derived winds from the CIRA-86, *J. Atmos. Sci.* **48,** 411–428.
Manson A. H., Meek C. E., Teitelbaum H., Vial F., Schminder R., Kurschner D., Smith M. J., Fraser, G. J. and Clark R. R.	1989	Climatologies of semi-diurnal and diurnal tides in the middle atmosphere (70–110 km) at middle latitudes (40°–55°) *J. atmos. terr. Phys.* **51,** 579–593.

Massebeuf M., Bernard R., Fellous J. L. and Glass M. 1979 The mean zonal circulation in the meteor zone above Garchy (France) and Kiruna (Sweden) *J. atmos. terr. Phys.* **41,** 647–655.

Massebeuf M., Bernard R., Fellous J. L. and Glass M. 1981 Simultaneous meteor radar observations at Monpazier (France, 44°N) and Punta Borinquen (Puerto-Rico, 18°N). II-Mean zonal wind and long period waves *J. atmos. terr. Phys.* **43,** 525–533.

Miyahara S., Portnyagin Y. I., Forbes J. M. and Solovjeva T. V. 1991 Mean zonal acceleration and heating of the 70- to 100-km region, *J. geophys. Res.*, **96,** 1225–1238.

Morse P. M. and Feshbach H. 1953 *Methods of Theoretical Physics*, McGraw-Hill, New York.

Oort A. H. 1983 Global atmospheric circulation statistics, 1958–1983, *NOAA Professional Paper* **14,** National Oceanic and Atmospheric Admin., p. 180, U.S. Government Printing Office, Washington, DC 20402.

Reed R. J., Oard M. J. and Sieminski M. 1969 A comparison of observed and theoretical diurnal tidal motions between 30 and 60 kilometers, *Mon. Weather Rev.* **97,** 456–459.

Salby M. L. and Roper R. G. 1980 Long-period oscillations in the meteor region, *J. Atmos. Sci.* **37,** 237–244.

Schmidlin F. J. 1986 Rocket techniques used to measure the neutral atmosphere *Handbook for Map*, **19,** Ed. R. A. Goldberg, Urbana, IL, 1–28.

Schmidlin F. J., Carlson M., Rees D., Offermann D., Philbrick C. R. and Widdel H. U. 1985 Wind structure and variability in the middle atmosphere during the November 1980 Energy Budget Campaign *J. atmos. terr. Phys.* **47,** 183–193.

Tsuda T., Nakamura T. and Kato S. 1987 Mean winds observed by the Kyoto meteor radar in 1983–1985 *J. atmos. terr. Phys.* **49,** 461–466.

Vincent R. A. and Stubbs T. J. 1977 A study of motions in the winter mesosphere using the partial reflection drift technique *Planet. Space Sci.* **25,** 441–445.

Vincent R. A. and Ball S. M. 1981 Mesospheric winds at low- and mid-latitudes in the southern hemisphere *J. geophys. Res.* **86,** 9159–9169.

Vincent R. A., Tsuda T. and Kato S. 1988 A comparative study of mesospheric solar tides observed at Adelaide and Kyoto, *J. geophys. Res.* **93,** 699–708.

Vincent R. A. and Lesicar D. 1991 Dynamics of the equatorial mesosphere: First results with a new generation partial reflection radar, *Geophys. Res. Lett.* **18,** 825–828,.

Vincent R. A., Tsuda T. and Kato S. 1989 Asymmetries in mesospheric tidal structure *J. atmos. terr. Phys.* **51,** 609–616.

Virdi T. S. and Williams P. J. S. 1989 Observations of tidal modes in the lower thermosphere using EISCAT, *Adv. Space Res.* **9**(5), 83–86.

Wand R. H. 1983 Seasonal variations of lower thermospheric winds from the Millstone Hill incoherent scatter radar *J. geophys. Res.* **88,** 9227–9241.